Electronic structure of ZnS, ZnSe, ZnTe, and their pseudobinary alloys

James E. Bernard and Alex Zunger
Solar Energy Research Institute, Golden, Colorado 80401
(Received 3 March 1987)

Using the all-electron mixed-basis approach to the density-functional formalism for crystals, we calculate from first principles the electronic structure of zinc-blende ZnS, ZnSe, and ZnTe as well as that of their ordered pseudobinary alloys Zn_2SSe, Zn_2SeTe, and Zn_2STe. For the latter we use as a model a CuAu I–like structure (space group $P\bar{4}m2$), and analyze the observed optical bowing in terms of three contributions: (i) a volume deformation of the band structure due to the replacement of the lattice constants of the binary constituents by that of the alloy, (ii) a chemical-electronegativity contribution due to charge exchange in the alloy relative to its constituent binary subsystems, and (iii) a structural contribution due to the relaxation of the anion-cation bond lengths in the alloy. The total bowing effect [the sum of (i)–(iii) above] agrees well with observations, yet the present analysis suggests a physical mechanism for optical bowing which differs profoundly from that offered by the popular virtual-crystal approach. The maximum contribution of disorder to the optical bowing is calculated for ZnS_xTe_{1-x} using a cluster-averaging method, resulting in a reduction in the bowing of the fundamental gap. We further discuss the band structures, x-ray scattering factors, charge distribution, and deformation potentials of the binary zinc chalcogenides and their ordered alloys.

I. INTRODUCTION: COMPOSITION DEPENDENCE OF SOME PROPERTIES OF PSEUDOBINARY SEMICONDUCTOR ALLOYS

A. Phenomenology

Soon after the development of modern techniques of crystal growth and purification of heteropolar binary semiconductors, it was realized that many pairs AC and BC of such semiconductors exhibit large ranges of mutual solid solubility, forming $A_xB_{1-x}C$ alloys.[1–4] It became apparent early on (see reviews of the early work in Refs. 1–4), that if both AC and BC belong to the same isostructural octet class (i.e., A and B are isovalent, and both AC and BC are III-V, or II-VI or I-VII), many of the physical properties of $A_xB_{1-x}C$ can be represented as a simple analytical interpolation of the properties of its constituent compounds (rather than viewing A_xB_{1-x} as a new chemical compound in its own right). Specifically, it was found that many physical properties $F(A_xB_{1-x}C)$ of such "pseudobinary" solid solutions could conveniently be related to the *linear* concentration (x) weighted average of the corresponding properties F_{AC} and F_{BC} of the endpoint compounds

$$\bar{F}(x)=xF_{AC}+(1-x)F_{BC} \tag{1a}$$

by simple quadratic relationships of the type

$$F(x)=\bar{F}(x)+kx(1-x)\ , \tag{1b}$$

where k is approximately composition independent (representing a general "bowing" parameter), and where by construction $F(1)=F_{AC}$ and $F(0)=F_{BC}$. X-ray diffraction experiments[1] have generally indicated no superlattice diffraction spots for high-temperature–grown alloys, showing that $A_xB_{1-x}C$ shares the same Bravais lattice as its components: With only a few (but significant[5]) exceptions, no structural phase transitions were observed as a function of composition. Diffraction experiments[1–4] have further revealed that within the underlying coherence length of the measurement (~ 1000 Å), the lattice constant $a(x)$ of the alloy is close to its concentration-weighted average

$$a(x)\cong xa_{AC}+(1-x)a_{BC}\equiv\bar{a}(x)\ , \tag{2}$$

i.e., for F the lattice constant, the bowing parameter of Eq. (1) is $k\cong 0$. (Small deviations from this Végard rule,[6] i.e., $k\neq 0$, have been observed for alloys with large lattice mismatches,[1] e.g., $In_xAl_{1-x}As$, $Ga_xAl_{1-x}Sb$, and $InSb_xAs_{1-x}$, and have been discussed by Fong *et al.*[7])

Optical experiments (see reviews in Refs. 4 and 8–11) have revealed that whereas incorporation of *nonisovalent* impurities B in a host crystal AC (e.g., Si:P, GaAs:Zn, or ZnS:Cu) produces new energy levels in the otherwise forbidden band gap, in most *isovalent* alloys no new states are formed, and instead the band edges move continuously with composition. (Exceptions include the isovalent impurity systems GaP:N and GaP:Bi, where the large size and electronegativity mismatch between A and B lead to the formation of bound states and to a limited solubility.[12]) However, in contrast to the tendency of $a(x)$ to stay close to its concentration average value $\bar{a}(x)$ [Eq. (2)], alloy band gaps $\varepsilon_g(x)$ were found to deviate considerably from their concentration-weighted average

$$\bar{\varepsilon}_g(x)=x\varepsilon_{AC}+(1-x)\varepsilon_{BC}\ . \tag{3}$$

In fact, most measurements of $\varepsilon_g(x)$ could be fit well to the form of Eq. (1), i.e.,

$$\varepsilon_g(x)=\bar{\varepsilon}_g(x)-bx(1-x) \tag{4}$$

with a nearly composition-independent "optical bowing parameter" b. Equations (3) and (4) show that $\varepsilon_g(x)$ attains an extremum at

TABLE I. Observed optical bowing parameters (in eV) for the direct band gap of pseudobinary ZnS, ZnSe, and ZnTe alloys. The growth method and the method used to measure the spectra are given in the footnotes.

ZnS_xSe_{1-x}	$ZnSe_xTe_{1-x}$	ZnS_xTe_{1-x}	Ref. and year
~0	1.28	2.40	Ref. 20 (1957)[a]
0.6			Ref. 23 (1963)[b]
		3.0	Ref. 27 (1973)[c]
	1.23		Ref. 29 (1972)[d]
0.41			Ref. 26 (1977)[e]
0.63			Refs. 21,22 (1979)[f]
0.43			Ref. 24 (1982)[g]
0.456			Ref. 25 (1985)[h]

[a]Bulk microcrystals produced by heating at 900 °C the powdered constituents; diffuse reflectance.
[b]Polycrystals producing by firing constituents in sealed quartz capsules at 950 °C; photoluminescence.
[c]Thin films prepared by evaporation; absorption.
[d]Single crystals, grown by a modified closed vapor-phase method; reflectivity.
[e]Melt-grown crystals; reflectivity.
[f]Epitaxial films grown on CaF_2 by vapor-phase reaction; spectra measured through the contact potential between the samples surface and reference (Kelvin) electrode.
[g]Single crystals grown by iodine transport.
[h]Polycrystalline thin films grown by evaporation; absorption.

$$x_m = \frac{1}{2}\left[1+\frac{\Delta\varepsilon}{b}\right] \tag{5}$$

(where $\Delta\varepsilon=\varepsilon_{BC}-\varepsilon_{AC}$), with an extremal value

$$\varepsilon_g(x_m)=(\varepsilon_{AC}+\varepsilon_{BC})/2+\Delta\varepsilon^2/4b-b/4\ . \tag{6}$$

For alloys with small band-gap mismatch $\Delta\varepsilon$, the extremum occurs at $x_m\cong\frac{1}{2}$. The optical bowing parameter b of the lowest band gap is usually found to be positive,[1-4,8-10] i.e., $\varepsilon_g(x)$ is concave upward; the extremum point $(x_m,\varepsilon_g(x_m))$ hence represents a minimum. ($Zn_xHg_{1-x}Se$ is an exception, showing[13] $b<0$ at small x. Likewise, the spin-orbit splitting of the top of the valence band often shows[14-18] $b<0$). Equations (5) and (6) show that alloys with large $\Delta\varepsilon$ and b can have a minimum gap $\varepsilon_g(x_m)$ lower than the smaller of ε_{AC} and ε_{BC}, and away from $x_m=\frac{1}{2}$. Perhaps the most striking example of optical bowing in isovalent semiconductor alloys is provided by solid solutions of zinc chalcogenides ZnS_xSe_{1-x}, $ZnSe_xTe_{1-x}$, and ZnS_xTe_{1-x}, all approximately adhering to Végard's rule[19] [Eq. (2)] in the range of their solid solubility, yet exhibiting some of the smallest bowing parameters [$b\sim0$–0.6 eV for ZnS_xSe_{1-x} (Refs. 20–27)] and the largest [$b\cong3.0$ eV for ZnS_xTe_{1-x} (Refs. 20 and 27)] ever observed in isovalent pseudobinary solutions. (For $ZnSe_xTe_{1-x}$, the bowing is about 1.3 eV.[20,28,29]) Table I summarizes the observed bowing parameters in these systems.

The phenomenological observations surrounding the composition dependence of $a(x)$ and $\varepsilon_g(x)$ have motivated investigations[30-40] into possible interrelationships between these quantities. Contemporary approaches to this question are discussed next.

B. Contemporary approaches to optical bowing

Attempts to find simple phenomenological linear relationships between the optical bowing $b(A_xB_{1-x}C)$ [Eq. (4)] and the lattice-constant mismatch $a_{AC}-a_{BC}$, band-gap mismatch $\varepsilon_{AC}-\varepsilon_{BC}$, or electronegativity difference $\chi_{AC}-\chi_{BC}$, have generally failed.[1,3] Nonetheless, the need to fine tune the band gaps $\varepsilon_g(x)$ of alloys in various device applications including light-emitting diodes, low-loss optical fibers, heterojunction lasers, infrared detectors, and solar cells, has provoked an interest in understanding optical bowing in terms of the properties of the constituent compounds AC and BC. The earliest and still the most prevailing approach to the problem has been the virtual-crystal approximation[41] (VCA), in which the identity of the individual A and B elements in the alloy is abandoned, replaced by an average ("virtual") element $\langle AB\rangle$. This approach has been applied to semiconductor alloys within the empirical pseudopotential method[30-37] (EPM), the dielectric two-band model (D2BM),[38-40] and the empirical tight-binding method.[17,42-44] The underlying Hamiltonian $\hat{H}$ considered in the VCA is

$$\begin{aligned}\hat{H}&=[-\nabla^2+V_{BC}(\mathbf{r})]+x[V_{AC}(\mathbf{r})-V_{BC}(\mathbf{r})]\\&=-\nabla^2+[xV_{AC}(\mathbf{r})+(1-x)V_{BC}(\mathbf{r})]\ ,\end{aligned} \tag{7}$$

where $V_{AC}(\mathbf{r})$ and $V_{BC}(\mathbf{r})$ are the periodic potentials of the pure AC and BC crystals *evaluated at the alloy lattice constant* $a(x)$. In what follows we describe some of the properties of this approach, and contrast them with experimental findings in semiconductor alloys.

(i) The perturbation $\Delta V(\mathbf{r})=V_{AC}(\mathbf{r})-V_{BC}(\mathbf{r})$ has the same periodicity as that of the underlying end-point compounds; it therefore couples the Bloch functions $\{\phi^{AC}_{n\mathbf{k}}(\mathbf{r})\}$ and $\{\phi^{BC}_{m\mathbf{k}}(\mathbf{r})\}$ of AC and BC, respectively, only at the wave vector $\mathbf{k}$ of the (common) Brillouin zone.

This conflicts with the observed relaxation of optical selection rules in alloys.[45] Coupling between these Bloch states can be introduced in second-order perturbation theory[46] and yields a correction

$$\sum_{m}\sum_{\mathbf{k}'} |\langle \phi_{n\mathbf{k}} | \Delta V | \phi_{m\mathbf{k}'} \rangle|^2/(\varepsilon_{n\mathbf{k}}-\varepsilon_{m\mathbf{k}'})$$

to the VCA eigenvalue $\varepsilon_{n\mathbf{k}}$.

(ii) Since, in addition, $\Delta V(\mathbf{r})$ also transforms like the totally symmetric representation of the point group of AC and BC, it cannot alter the symmetry representation (hence, orbital character) of the alloy band wave functions relative to that of AC and BC. For example, the Γ_{15v} state (a p-d orbital, forming the top of the valence band in zinc-blende semiconductors) cannot mix with the Γ_{1c} state (a predominantly s-type orbital in the conduction band). However, the observed bowing of the spin-orbit splitting[14–18] indicates[16,17] an alloy-induced mixing of s character into the top of the valence band.

(iii) Since the identities of atoms A and B, including the characteristic electronegativities and scattering powers towards electron orbits of given angular momenta (reflected, for example, in the shape of their l-dependent pseudopotentials), are abandoned in the VCA in favor of an average species [Eq. (7)], *direct* chemical events between AC and BC (e.g., charge redistribution and polarization[47,48(a)]) are precluded as well. In fact, a chemical disparity between $V_{AC}(\mathbf{r})$ and $V_{BC}(\mathbf{r})$ could lead to the preferential localization of an alloy wave function on one sublattice, splitting thereby the degeneracy mandated by VCA (where both A and B share the same potential). Such is the case in $Hg_xCd_{1-x}Te$ alloys, where the different attractiveness of $V_{Hg}(\mathbf{r})$ and $V_{Cd}(\mathbf{r})$ towards $l=0$ waves (Hg having a deeper outer s electron than Cd) results in an observed splitting[49] between the Hg and Cd valence s bands. The same effect has been observed[50] in ZnS_xSe_{1-x}, where the different potentials $V_S(\mathbf{r})$ and $V_{Se}(\mathbf{r})$ result in distinct ZnS-like and ZnSe-like features in the alloy's reflectivity spectra and in exciton localization in $ZnSe_xTe_{1-x}$.[51] Such is also the case for Raman scattering of phonons,[52] impurity photoluminescence in alloys,[53,54] or nuclear-magnetic-resonance studies,[55] which have revealed distinctly different chemical environments for Cd and Hg in $Hg_{1-x}Cd_xTe$. The neglect of this effect in VCA is often referred to as the neglect of "chemical disorder".

(iv) In its application to alloys whose constituents have more than one type of atom in the unit cell (e.g., AC and BC), a specification of bond lengths is required (in addition to the lattice constant a) to solve for the spectrum of $\hat{H}$. Practitioners of the VCA in pseudobinary alloys have often assumed[30–40,42–46] also the "virtual-lattice model" (VLM), i.e., that the same geometrical relationship that exists in pure AC and BC compounds between the bond lengths (R_{AC} and R_{BC}) and the lattice constants a_{AC} and a_{BC} [e.g., $R_{\alpha\beta}=(\sqrt{3}/4)a_{\alpha\beta}$ in the zinc-blende structure] continues to hold in the alloy. Since the identity of the A and B sublattices is abandoned in the VCA in favor of a "virtual" average sublattice $\langle AB \rangle$, the VLM suggests that

$$R_{AC}(x)=R_{BC}(x)\equiv R_{\langle AB\rangle C}(x)=\lambda a(x) , \quad (8)$$

where λ is a geometrical constant (e.g., $\sqrt{3}/4$ in the zinc-blende structure). This is equivalent to the statement that Végard's rule applies not only to atomic volumes [Eq. (2), as is suggested by Végard], but also to bond lengths (not implied by Végard[6]). This is often referred to as the neglect of "positional disorder," or the postulation of a "unimodal distribution of bond lengths." It has been pointed out,[56] however, that Eq. (2) does not require Eq. (8) to hold: simple three-dimensional networks can be constructed[48(a)] such that for *any* prescribed $a=a(x)$, two arbitrarily dissimilar bond lengths R_{AC} and R_{BC} can coexist. Such is the case in the chalcopyrite structure of $A^{I}F^{III}C_2^{V}$ compounds (where,[57] in $CuInSe_2$, one has $R_{CuSe}\neq R_{InSe}$), or the CuAu I structure.[47,58,59] Indeed, extended x-ray-absorption fine structure (EXAFS) experiments[60,61] and valence-force-field calculations[62] indicate substantial bond alternation [$R_{AC}(x)\neq R_{BC}(x)$] in pseudobinary alloys.

(v) Implicit in Eq. (7) is also the requirement that the effective potential of the alloy be *linear* in the effective potentials of its constituents. This "superposition approximation" limits the classes of electronic structure methods which are accessible through Eq. (7): they need be both *valence-electron methods* (since core states cannot be averaged) such as pseudopotential,[30–37] tight-binding[42–44] or dielectric models,[38–40] and *linear* models (e.g., the *empirical* pseudopotential method, but not the *self-consistent* pseudopotential method). This is so because the empirical pseudopotential method[63] postulates that *screened* atomic pseudopotentials are superposable, whereas self-consistent pseudopotential methods[64] assume a superposition of only the ionic pseudopotentials, recognizing that screening effects are not linearly superposable. These inherent restrictions of Eq. (7) have severely hampered the sophistication with which previous approaches were able to describe the electronic structure of semiconductor alloys.

C. Why VCA models produce optical bowing

The basic reason why VCA Hamiltonians of the type described in Eq. (7) can produce a nonzero bowing parameter [Eq. (4)] despite the use of a *linear* average of potentials is the fact that most band-structure methods produce eigenvalues that are nonlinear in the potential matrix elements. If V_A, U_A, and W_A denote general potential parameters of a given crystal A, in general, the band structure energies $\varepsilon_A^{(i)}$ of the crystal A at its equilibrium lattice constant a_A have nonlinearities of the form

$$\varepsilon_A^{(i)}=\alpha V_A(a_A)+\beta U_A^2(a_A)+\gamma W_A^3(a_A)+\cdots . \quad (9)$$

In empirical methods,[38,63,65] $\{V_A, U_A, W_A, \ldots\}$ for their combinations are treated as disposable parameters used to fit $\varepsilon_A^{(i)}$. Such is the case in the empirical pseudopotential method,[63] where, for example, the band gap at

the X point in the zinc-blende Brillouin zone is approximately given by[65]

$$\varepsilon_X \cong 2V(220)+\frac{a^2}{2\pi^2}V^2(111) \tag{10}$$

[where $V_A=V(220)$ and $U_A=V(111)$ are pseudopotential form factors]. Such is also the case in the simple tight-binding method,[66] where the band energies at high-symmetry points have the form

$$\varepsilon_A^{(i)}=V_A\pm(U_{1A}^2+U_{2A}^2)^{1/2}=\begin{cases} V_A\pm U_{1A}\pm\frac{1}{2}U_{2A}\dfrac{U_{2A}}{U_{1A}}+\cdots, & U_{1A}>U_{2A} \\ V_A\pm U_{2A}\pm\frac{1}{2}U_{1A}\dfrac{U_{1A}}{U_{2A}}+\cdots, & U_{2A}>U_{1A} \end{cases} \tag{11}$$

(V_A and U_A being Hamiltonian matrix elements). In the dielectric two-band model,[38] we have a similar situation, where the effective band gap is

$$\varepsilon_A^{(i)}=(V_A^2+U_A^2)^{1/2}=\begin{cases} V_A+\frac{1}{2}U_A\dfrac{U_A}{V}+\cdots, & U_{1A}>U_{2A} \\ U_A+\frac{1}{2}V_A\dfrac{V_A}{U_A}+\cdots, & U_A>V_A \end{cases} \tag{12}$$

(where V_A and U_A are homopolar and heteropolar gaps, respectively). The nonlinearity of the energies $\varepsilon_A^{(i)}$ with respect to the potential parameters underlying all of these methods *guarantees* a nonzero bowing in the VCA. Expressing the VCA band gap from Eq. (9) for the *alloy* lattice constant $a=a(x)$ as

$$\varepsilon_g^{\mathrm{VCA}}(x)=\alpha[xV_{AC}(a)+(1-x)V_{BC}(a)] +\beta[xU_{AC}(a)+(1-x)U_{BC}(a)]^2+\cdots, \tag{13}$$

one gets from Eqs. (3), (4), and (13) the general result

$$b_{\mathrm{VCA}}=\{\bar{\varepsilon}-[\alpha\bar{V}(a)+\beta\bar{U}^2(a)]\}/x(1-x), \tag{14a}$$

where

$$\begin{aligned} \bar{V}(a)&=xV_{AC}(a)+(1-x)V_{BC}(a), \\ \bar{U}(a)&=xU_{AC}(a)+(1-x)U_{BC}(a), \end{aligned} \tag{14b}$$

and $\bar{\varepsilon}=\bar{\varepsilon}(a_{AC},a_{BC})$ is given by Eq. (3). If one uses a single lattice constant $a=a(x)$ in Eq. (14b), as done by Hill and Richardson,[35] one finds

$$b_{\mathrm{VCA}}=\beta[U_{AC}(a)-U_{BC}(a)]^2+\cdots, \tag{15a}$$

whereas if the lattice constants of the end-point compounds are used,[38] one has

$$b_{\mathrm{VCA}}=\beta[U_{AC}(a_{AC})-U_{BC}(a_{BC})]^2+\cdots. \tag{15b}$$

This shows that b_{VCA} is given by the square of the difference in the nonlinear potential parameters of the two end-point crystals, *evaluated at an interpolated lattice constant $a(x)$ of the alloy*. Regrettably, this is not a very compelling relationship: it has been amply demonstrated in the literature[67] that by using semiempirical band-structure models it is possible to fit almost equally well a given set of band energies by widely different choices of the potential parameters. Since the informational content of the observed bowing curves $\varepsilon_g(x)$ [Eq. (4)] is but one number per transition (i.e., b), we were able to obtain through Eqs. (14b) and (15a) almost *any* desired bowing parameter b_{VCA} by a suitable choice of interpolated $U_{AC}(a(x))$ and $U_{BC}(a(x))$ values, without spoiling the fit of the band structure of the end-point compounds (at $a=a_{AC}$ and $a=a_{BC}$) to experiment. This can be demonstrated by expanding the expressions for band gaps into a Taylor series of the form in Eq. (9) [e.g.,[66] Eqs. (11) and (12)]. It then becomes apparent that the nonuniqueness[67] of the nonlinear terms permits almost any value of b_{VCA} [Eq. (14a)].

Previous efforts to calculate the bowing parameters for zinc chalcogenide alloys[33–39] were based on the VCA approach within the dielectric two-band model[38–39] or the empirical pseudopotential method.[33–37] A summary of some values of b obtained in D2BM and EPM models for the alloys discussed in this paper is given in Table II.

D. Role of order and disorder

It is useful to separate the observed bowing parameters b_{expt} into a contribution b_{I} due to order effects which exist already in a fictitiously periodic alloy, and a contribution b_{II} due to disorder effects[38]

$$b_{\mathrm{expt}}=b_{\mathrm{I}}+b_{\mathrm{II}}. \tag{16}$$

TABLE II. Calculated optical bowing parameters (in eV) for the direct band gap of Zn chalcogenide alloys.

	VCA-D2BM[a]				VCA-EPM[b]
Alloy	b_{I}	b_{II}	$b_{\mathrm{expt}}-b_{\mathrm{I}}$	b_{expt}	b_{I}
ZnS_xSe_{1-x}	0.14	0.14	~ 0.32	0.46	0.60
$ZnSe_xTe_{1-x}$	-0.04	1.14	~ 1.27	1.23	0.90
ZnS_xTe_{1-x}	0.28	2.12	~ 2.72	3.0	3.02
$Ga_xIn_{1-x}P$	0.39	0.31			

[a]Dielectric two-band model [Eq. (12)] of Van Vechten and Bergstresser, Ref. 38.
[b]Empirical pseudopotential method [Eqs. (10)–(15)] of Richardson, Ref. 36.

In the past, b_{I} has been described largely by empirical VCA models.[30–40,42–44] The contribution of disorder, taken as the amount by which b_{I} fails to account for the observed $b=b_{\mathrm{expt}}$, was either modeled empirically,[38] described by second-order perturbation theory for compositional disorder,[46] or by the difference $b_{\mathrm{II}}\cong b_{\mathrm{CPA}}-b_{\mathrm{VCA}}$ between the bowing parameter b_{CPA} obtained in the coherent-potential approximation[68–71] (CPA), including compositional disorder effects, and that obtained in VCA calculations ($b_{\mathrm{VCA}}=b_{\mathrm{I}}$). The VCA calculation of Van Vechten and Bergstresser[38] (Table II), utilizing the dielectric two-band model, showed that VCA effects for these systems account only for a small part of b_{expt} (Table II), leaving a large portion $b_{\mathrm{expt}}-b_{\mathrm{I}}$ to be described by disorder phenomena. Subsequent CPA calculations[68–71] do not warrant ascribing such a dominant role to compositional disorder, e.g., $(b_{\mathrm{CPA}}-b_{\mathrm{VCA}})/b_{\mathrm{CPA}}=3\%$ for $Ga_xIn_{1-x}P$,[68] whereas b_{II} of Van Vechten and Bergstresser[38] for $ZnSe_xTe_{1-x}$ and ZnS_xTe_{1-x} is overwhelmingly significant over b_{I} (Table II). It is indeed difficult to grant such a decisive role to disorder effects (as concluded from comparing b_{expt} to b_{VCA}) in view of the remarkably sharp Raman lines,[52] crystal-like reflectivity spectra[8,21] (with sharp edges), and high electron mobilities[72] often observed in these alloys. (CPA calculations have indeed considerably rectified this situation, explaining the narrow linewidths and high mobilities in the presence of compositional disorder.)

The ambiguities discussed above in the calculated b_{VCA} (and indeed, their large spread, cf. Table II) make it impossible to assess clearly the roles of chemical interactions, structural relaxations and genuine disorder effects. Furthermore, the success in interpreting experiment through VCA models and the resulting conclusions on decisive disorder effects is ambiguous. Consider the following examples.

(i) Van Vechten *et al.*[16] argued that the observed (negative) bowing of the spin-orbit coupling provides conclusive proof of the role of disorder, since in VCA the top of the valence band (Γ_{15v}) is a pure non-s state, and consequently it cannot lead to s-p mixing and hence negative bowing of the spin-orbit splitting [see item (ii) in Sec. I B]. They showed that phenomenological disorder models can mix s character into the top of the valence band, thus explaining their bowing. However, mixing of s character into the Γ_{15v} state is possible by other mechanisms as well: It exists, for example in *ordered crystalline* chalcopyrite systems[56,57] ABC_2, simply since the anion C is coordinated (in a coherent fashion) by two A and two B atoms. This symmetry lowering (incorporated naturally in our calculations, see Sec. III B) permits s-p mixing.

(ii) Pearsall[40] found a good agreement between his measured bowing and the phenomenological model of Van Vechten and Bergstresser[38] associating disorder with the square of the difference of the electronegativities of the alloyed atoms. This too, however, does not constitute any proof of the relevance of disorder, since the order contribution b_{I} also scales with the electronegativity difference[56–57] (see also discussion in Sec. VI).

(iii) Similarly, the perturbation argument of Baldereschi and Maschke[46(a)] suggesting the importance of compositional disorder in GaP_xAs_{1-x} is also not compelling: Interband mixing, of the sort included in their calculation can exist in part also in ordered superstructures, where the Brillouin zone is folded (see Sec. III C below).

We conclude that existing VCA-based calculations for semiconductor alloys do not provide a sound basis for assessing the relative significance of order and disorder effects. In what follows, we describe an alternative approach to the calculation of b_{I}.

II. MICROSCOPIC MODEL FOR b_{I}

A. The basic idea

We imagine the tetrahedrally coordinated $A_xB_{1-x}C$ alloy to consist at each composition x and temperature T of the basic tetrahedral units CB_4 (as in BC), CAB_3, CA_2B_2, CA_3B, and CA_4 (as in AC) (i.e., $n=0$, 1, 2, 3, and 4 A atoms, respectively) with a distribution function $P^{(n)}(x,T)$ for each "subcrystal" n. Each of these fourfold-coordinated structural units can be thought of as the repeat unit of a periodic structure $A_nB_{4-n}C_4$. Whereas the binary systems AC ($n=4$) and BC ($n=0$) have, in their zinc-blende form, just a single (external) degree of freedom [the lattice constants a_{AC} and a_{BC}, which uniquely determine the bond lengths $R_{AC}=(\sqrt{3}/4)a_{AC}$ and $R_{BC}=(\sqrt{3}/4)a_{BC}$], the ternary systems $n=1$, 2, and 3 can have cell internal degrees of freedom as well, denoted collectively as $\{u^{(n)}\}$. In these systems the internal parameters allow the bond lengths to relax toward their (natural) zinc-blende values, and the expressions for the bond lengths $R_{AC}^{(n)}$ and $R_{BC}^{(n)}$ then no longer have the simple (ideal) form found in the zinc-blende structure [Eq. (26)]. At equilibrium, a crystal

composed of a single type of cluster $A_nB_{4-n}C_4$ would be characterized by the lattice constants $a_{\rm eq}^{(n)}$ and $c_{\rm eq}$, and (for $n=1$, 2, or 3) the internal structural parameters $\{u_{\rm eq}^{(n)}\}$, with corresponding bond lengths. In the alloy, however, we make the assumption that all five types of clusters have the lattice constant $a^{(n)}(x)=a(x)$ appropriate for the alloy. The relaxed internal parameters are then $u^{(n)}(x)=u^{(n)}(a(x))$ (i.e., dependent on the composition of the alloy), and the corresponding bond lengths are $R_{AC}^{(n)}(x)=R_{AC}^{(n)}(a(x))$ and $R_{BC}^{(n)}(x)=R_{BC}^{(n)}(a(x))$. The formation of each subcrystal at the alloy lattice constant, with relaxed internal parameters, from the end-point compounds AC and BC at their equilibrium lattice constants can be described by the formal chemical reaction

$$n[AC,a_{AC}]+m[BC,a_{BC}]\rightleftarrows[A_nB_mC_{n+m},a(x),u^{(n)}(x)]\ . \tag{17}$$

The probability distribution $P^{(n)}(x,T)=P^{(n)}(x(a),T)$ can be calculated from Kikuchi's cluster variation method[73] if the changes in internal energies accompanying reaction (17) are known[74] (or else can be approximated as a random distribution[48(a)]). Denoting by $\varepsilon_{ABC}^{(i,n)}(a(x),u^{(n)}(x))$ the ith interband transition energy (i.e., fundamental, or any other band gap) of the subcrystal $A_nB_mC_{n+m}$, its optical bowing parameter is given by Eq. (4) as

$$b^{(i,n)}=\frac{(m+n)^2}{mn}\left[\frac{n}{m+n}\varepsilon_{AC}^{(i,4)}(a_{AC})+\frac{m}{m+n}\varepsilon_{BC}^{(i,0)}(a_{BC})-\varepsilon_{ABC}^{(i,n)}(a(x),u^{(n)}(x))\right]\ . \tag{18}$$

The effective interband transition energies of the mixed alloy could be modeled as an average of $\varepsilon_{ABC}^{(i,n)}$ over the probabilities $P^{(n)}(x(a),T)$. Our program is somewhat more modest than this. Since at a fixed concentration x (say, $x=\frac{1}{2}$) $P^{(n)}(x,T)$ shows a maximum occurrence[48,74] of the species whose n best represents the composition (e.g., a 50%-50% compound ABC_2 at $x=\frac{1}{2}$), and since calculations on $Al_nGa_mAs_{n+m}$ (Ref. 58) and $Ga_nIn_mP_{n+m}$ [Ref. 48(a)] show a weak dependence of $b^{(i,n)}$ on n (i.e., $AlGaAs_2$, $AlGa_3As_4$, and Al_3GaAs_4 have different band structures but similar bowing of the same transition i), we will first limit our discussion to a single subcrystal $m=n=2$ (Fig. 1), corresponding to the majority species $A_2B_2C_4=2ABC_2$ at $x=\frac{1}{2}$. The effects of the *minority species* (e.g., A_3BC_4 and AB_3C_4 at $x=0.5$) will then be added. The bowing parameter calculated for $n=2$ corresponds to the actual case for $x=\frac{1}{2}$ at temperatures below the ordering temperature T_O; we expect it to be a reasonable approximation for temperatures just above T_O. We will hence first calculate $b^{(i,2)}$ from Eq. (18) by performing band-structure calculations for AC, BC, and ABC_2. Such a calculation of $b^{(i)}$ corresponds to the "order" component [$b_{\rm I}$ in Eq. (16)] of the bowing, leaving out genuine disorder effects; deviations of $b_{\rm I}$ from experiment will be used, among others, to judge the significance of disorder effects $b_{\rm II}$. However, contrary to previous VCA calculations,[30–44] we will retain the identity of the two different sublattices A and B. This will allow us to incorporate into $b_{\rm I}$ most of the effects ignored previously [i.e., items (ii)–(iv) in Sec. I B].

In performing such band calculations on ordered alloy models, a structural unit $A_nB_mC_{n+m}$ is required. We choose the unit such that each sublattice (AC and BC) has the same fcc Bravais lattice as in the end-point compounds, consistent with EXAFS data.[60,61] The choice of such structural units is best based on the Landau-Lifshitz theory of order-disorder transformations,[75,76] adapted to two fcc sublattices.[47,74] This theory allows us to select structures with the following properties: (i) they are the only ones where the order-disorder transformation *can* (but need not) be of second order,[75] (ii) all of these structures (and no others) are stable against antiphase boundaries,[76] and (iii) they can exist over a wide concentration range.[76] For *ternary* $A_nB_mC_{n+m}$ adamantine semiconductors (with disorder on two fcc sublattices), there are eight Landau-Lifshitz structures,[48(a),47] including, for the 50%-50% structure ABC_2 the CuAu I–like (simple tetragonal, $P\bar{4}m2$, or D_{2d}^5, Fig. 1) and chalcopyrite (centered tetragonal, $I\bar{4}2d$, or D_{2d}^{12}), as well as two structures for the 25%-75% case of A_3BC_4 and AB_3C_4, namely a Cu_3Au-like structure (the cation sublattice is like that of Cu_3Au, the lattice is simple cubic, the space group is $P\bar{4}3m$ or T_d^1, and the structure is like that of Fig. 1 but with the A atom at the center of each horizontal plane replaced by a B atom), and famatinite (centered tetragonal, $I\bar{4}2m$ or

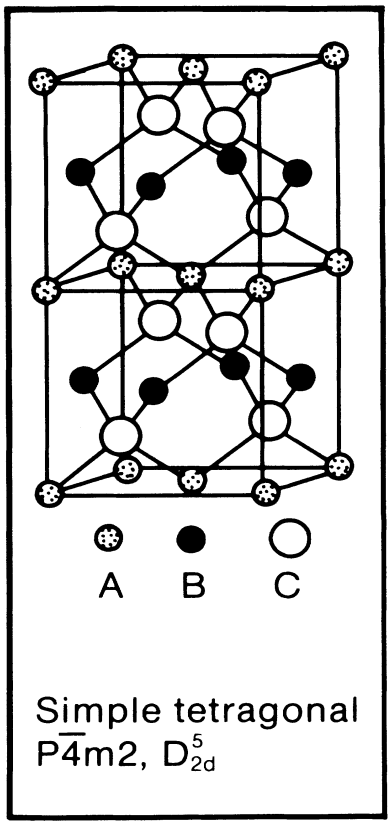

FIG. 1. Crystal structure of ABC_2.

D_{2d}^{11}). Srivastava *et al.*[48(a)] have previously performed total-energy calculations for $Ga_nIn_mP_{n+m}$ in these Landau-Lifshitz structures. Here, for simplicity we will represent the 50%-50% alloy by the $n=2$ structure with the smallest unit cell: the four-atom CuAu I–like structure which is expected to be representative of structures where the C atom is bonded by two A and two B atoms. In contrast to the more complex chalcopyrite structure we have used previously,[48(a),56,57] the CuAu I structure has along its c axis the same type of atom, hence it is not naturally birefringent (indeed, a disordered cubic alloy is likewise optically isotropic). (Note[58] that the CuAu I structure is equivalent to a (1,1) monolayer superlattice of $AC+BC$ in the [001] direction.) Using it as the structural unit for our alloy model will hence make it possible to use known superlattice effects to discuss optical bowing in alloys. For example, the folding of the X point of the zinc-blende Brillouin zone into the Γ point of the CuAu I Brillouin zone (see Sec. III C) makes it natural to interpret no-phonon (pseudo-) direct absorption lines observed[45] in alloys. Furthermore, the band-gap change as the ABC_2 "superlattice" is formed from $AC+BC$ is naturally interpretable as a superlattice shift of nearly confined band states. The corrections to the bowing due to the existence of other structures (AC, BC, A_3BC_4, and AB_3C_4) at $x=0.5$ will then be added, using the zinc-blende (for AC and BC) and Cu_3Au-like structures (for A_3BC_4 and AB_3C_4). Note that such chalcopyrite, CuAu I and famatinite *ordered* structures are *observed* in isovalent semiconductor alloys.[77]

B. Decomposition of b_1 into three physical contributions

To gain insight into the microscopic mechanism controlling optical bowing, we follow Zunger and Jaffe,[56,57] Martins and Zunger,[78] and Srivastava *et al.*,[48(a)] and decompose the overall process of Eq. (17) into three steps, each calculated separately for the $n=2$ cluster.

First, we compress and dilate the lattice constants of AC and BC into that $a(x=0.5)\cong a_{\rm eq}^{(2)}$ pertinent to the 50%-50% alloy, i.e., we perform the formal reactions

$$[AC,a_{AC}]\rightarrow[AC,a(0.5)]$$

and (19a)

$$[BC,a_{BC}]\rightarrow[BC,a(0.5)]\ ,$$

yielding a volume-deformation (VD) contribution

$$b_{\rm VD}^{(i)}=2[\varepsilon_{AC}^{(i)}(a_{AC})+\varepsilon_{BC}^{(i)}(a_{BC})] -2[\varepsilon_{AC}^{(i)}(a(0.5))+\varepsilon_{BC}^{(i)}(a(0.5))] \quad (19b)$$

to the optical bowing. Although we calculate $b_{\rm VD}$ directly from the band structure, this contribution could also be calculated from the observed hydrostatic band-gap deformation potentials[79] $\gamma_{AC}^{(i)}=d\varepsilon_{AC}^{(i)}/d\ln\Omega_{AC}$ (where Ω_{AC} is the unit cell volume) of the pure compounds AC and BC. This yields

$$b_{\rm VD}^{(i)}=6\ln\left[\frac{a_{AC}^{\gamma_{AC}}a_{BC}^{\gamma_{BC}}}{a^{(\gamma_{AC}+\gamma_{BC})}}\right]\ . \quad (19c)$$

Hence $b_{\rm VD}^{(i)}$ simply represents the relative response of the band structures of AC and BC to (positive and negative) hydrostatic pressures.

Second, we bring together AC and BC, "prepared" at the common lattice constant $a(0.5)$, to form the ABC_2 compound, without relaxing the internal degrees of freedom (i.e., keeping $R_{AC}=R_{BC}$, just like in the VLM, denoted here as "unrelaxed" bonds, or "unrel"). The formal reaction is

$$[AC,a(0.5)]+[BC,a(0.5)]\rightarrow[ABC_2,a(0.5),u_{\rm unrel}^{(2)}]\ . \quad (20a)$$

At this stage, the AC and BC bonds can communicate through charge redistribution, reflecting a possible chemical electronegativity (CE) difference. The contribution of this reaction to the bowing is hence

$$b_{\rm CE}^{(i)}=2[\varepsilon_{AC}^{(i)}(a(0.5))+\varepsilon_{BC}^{(i)}(a(0.5))] -4\varepsilon_{ABC_2}^{(i)}(a(0.5),u_{\rm unrel}^{(2)})\ . \quad (20b)$$

This term, among others, accounts for the fact that the point-ion Madelung energy of ABC_2 differs from that of AC and BC at the same bond lengths. This is so because the C-atom charge is different in AC and BC, but in ABC_2 there is a single type of C atom, hence a single C-atom charge. These differences in Madelung energies affect the band structure and contribute to $b_{\rm CE}$.

In the *third* step, we allow the internal degrees of freedom $\{u^{(2)}\}$ to attain their relaxed (i.e., equilibrium) values,

$$[ABC_2,a(0.5),u_{\rm unrel}^{(2)}]\rightarrow[ABC_2,a(0.5),u_{\rm eq}^{(2)}]\ . \quad (21a)$$

The contribution of this structural (S) equilibration to the bowing is hence

$$b_{\rm S}^{(i)}=4\varepsilon_{ABC_2}^{(i)}(a(0.5),u_{\rm unrel}^{(2)}) -4\varepsilon_{ABC_2}^{(i)}(a(0.5),u_{\rm eq}^{(2)})\ . \quad (21b)$$

A relaxation of the *internal* degrees of freedom is equivalent to a "frozen phonon."[80] Notice that this structural deformation can induce a charge rearrangement too (a polarization effect[48(a)]). If charge rearrangement attendant upon such a deformation in the alloy could be neglected, $b_{\rm S}^{(i)}$ could be evaluated in principle from *phonon* deformation potentials *of the constituents*[81] and the knowledge of $u_{\rm eq}^{(2)}-u_{\rm unrel}^{(2)}$ in the alloy. However, polarization effects induced by such structural deformations may be large (and may, in fact, change the sign of $b_{\rm S}$ calculated without them). We hence calculate $b_{\rm S}$ (as well as $b_{\rm VD}$ and $b_{\rm CE}$) directly from the self-consistent band structure.

The sum of the reactions of Eqs. (19a), (20a), and (21a) gives the net reaction

$$[AC,a_{AC}]+[BC,a_{BC}]\rightarrow[ABC_2,a(0.5),u_{\rm eq}^{(2)}]\ , \quad (22a)$$

and the corresponding total bowing [sum of Eqs. (19b), (20b), and (21b)]

$$b^{(i)}=2[\varepsilon_{AC}^{(i)}(a_{AC})+\varepsilon_{BC}^{(i)}(a_{BC})] -\varepsilon_{ABC_2}^{(i)}(a(0.5),u_{\rm eq}^{(2)})\ , \quad (22b)$$

as in Eqs. (4) and (18). This provides a model for $b^{(i)}$ in terms of three microscopically defined quantities

$$b_{\mathrm{I}}^{(i)} = b_{\mathrm{VD}}^{(i)} + b_{\mathrm{CE}}^{(i)} + b_{\mathrm{S}}^{(i)} , \tag{23}$$

i.e., a hydrostatic effect on the band structure, a charge exchange at constant bond lengths, and an internal structural relaxation effect. Each term is calculated separately from a self-consistent band-structure model to be described next.

III. DETAILS OF CALCULATION

A. Band structures

We use the self-consistent potential-variation mixed-basis (PVMB) band-structure method of Bendt and Zunger.[82] (Plane-wave pseudopotential methods converge unacceptably slowly for systems with bound $3d$ orbitals such as those encountered in Zn chalcogenides.) The crystal potential is represented by the nonrelativistic local-density formalism, using the exchange-correlation functional of Ceperley and Alder[83] as parametrized by Perdew and Zunger.[84] The basis set consists of a combination of symmetrized plane waves and localized orbitals. The latter are obtained numerically by solving a renormalized atom problem for the Zn, S, Se, and Te atoms using the same density functional utilized for the crystal, but confining the atoms into a Wigner-Seitz cell with radii of 2.24, 1.88, 2.06, and 2.32 a.u. for Zn, S, Se, and Te, respectively. Hamiltonian matrix elements are computed within this mixed basis with no shape approximations. We find that practically no precision is lost if we freeze the core orbitals $1s$, $2s$, and $2p$ for Zn and Se (the $3s$ and $3p$ *cannot* be frozen without substantial loss of precision), $1s$ for S, and $1s$, $2s$, $3s$, $2p$, $3p$, and $3d$ for Te. Special care is taken to represent the two crystal structures used here—zinc blende and CuAu I—*equivalently*: since the optical bowing is calculated as a difference between the band structures of these two different crystal structures, it is imperative that all be represented computationally to within the same (perfect or imperfect) precision. For example, at the limit $A=B$, the band structure AAC_2 in the CuAu I structure (four atoms per cell) must be numerically equal to the (folded) band structure of AC in the zinc-blende structure (two atoms per cell). This can be assured if (i) the same localized-orbital basis set is used for all structures, (ii) the plane wave bases have the same kinetic energy cutoff [i.e., $(G/2a)^2$], where G is the maximum momentum] in all structures and for all lattice constants used (rather than the same number of basis functions), and (iii) *equivalent* (i.e., those obtained by folding) $\mathbf{k}$ points (rather than any *special* $\mathbf{k}$ points) are used for all structures. We sample the Brillouin zone by using the special $\mathbf{k}$ points $(2\pi/a)(\frac{1}{4},\frac{1}{4},\frac{1}{4})$ (weight $\frac{1}{4}$), $(2\pi/a)(\frac{1}{4},\frac{1}{4},\frac{3}{4})$ (weight $\frac{3}{4}$) for the zinc-blende lattice, and the *equivalent* $\mathbf{k}$ points $(2\pi/a)(\frac{1}{4},\frac{1}{4},\frac{1}{4})$ (weight $\frac{1}{2}$) and $(2\pi/a)(\frac{3}{4},\frac{1}{4},\frac{1}{4})$ (weight $\frac{1}{2}$) for the CuAu I lattice, and $(2\pi/a)(\frac{1}{4},\frac{1}{4},\frac{1}{4})$ (weight 1) for the Cu_3Au-like lattice. In addition, the density of fast-Fourier-transform points per unit volume[82] is kept similar in all cases. These constructs are tested by performing a band-structure calculation of AC both in the zinc-blende and in the CuAu I (i.e., AAC_2) structures obtaining the same band eigenvalues.

Our coordinate-space basis set consists of 9, 4, 9, and 9 localized (numerically optimized) orbitals for Zn, S, Se, and Te, respectively. The kinetic energy cutoff for the plane-wave basis is such that 208, 241, and 296 plane waves are included for ZnS, ZnSe, and ZnTe, respectively, 443, 530, and 501 plane waves are included for Zn_2SSe, Zn_2SeTe, and Zn_2STe, respectively, and 1003 plane waves are included for Zn_4S_3Te and Zn_4STe_3 at the alloy $a(0.5)$ lattice constants. The total basis set size is hence 221, 259, 314, 474, 566, 532, 1060, and 1070 basis functions for ZnS, ZnSe, ZnTe, Zn_2SSe, Zn_2SeTe, Zn_2STe, Zn_4S_3Te, and Zn_4STe_3, respectively. To diagonalize these large Hamiltonian matrices we use the residual minimization method[85] which requires a direct diagonalization of only small matrices (100–300), does not require storage of the full Hamiltonian matrix, and produces eigensolutions to within a prescribed tolerance (usually a residual around 10^{-5}) with a computational effort *linearly* proportional to the number of eigensolutions sought (usually valence plus a few conduction bands), rather than to a third power of the total matrix size as common in Householder-Choleski methods. Self-consistency in the potential is obtained within a tolerance of 0.3 mRy. The self-consistency iteration cycle is accelerated significantly by use of the Jacobian update method.[82] The number of fast-Fourier-transform points ranges between 4096 and 19 683 (depending on structure and volume). With these computational parameters we achieve an overall precision of ~ 0.1–0.2 eV for core states, ~ 0.03 eV for valence states, and ~ 0.03 eV for conduction states.

The local-density approximation which we use is known[86] to underestimate significantly the band gaps of nonmetals if the latter are estimated from band eigenvalues rather than from total energies. We have, however, formulated the problem in such a way [Eq. (18)] that *absolute* band gaps are not needed, but rather their *differences* [Eqs. (19b), (20b), and (21b)] or pressure derivatives [Eq. (19b)] appear. Such quantities can be obtained within the local-density approach to a far better accuracy than the band gaps themselves.[57]

B. Evaluation of structural parameters

The evaluation of Eqs. (19b), (20b), and (21b) requires knowledge of the lattice constants a_{AC} and a_{BC} of the end-point compounds, that $[a(0.5)]$ of the ABC_2 system, as well as c/a and $u_{\mathrm{eq}}^{(2)}$. We obtain these as follows. We use the experimental lattice constants for the zinc-blende compounds (given in Table III). Since Végard's rule is satisfied reasonably well by the Zn chalcogenide alloys,[19] we use for $a(0.5)$ the average of the end-point compounds, also given in Table III.

We model the ABC_2 compound by the CuAu I structure (Fig. 1) having the unit cell vectors

TABLE III. Lattice parameters, cation displacement parameter [Eq. (29)], and bond lengths for 50%-50% alloys, as obtained from an elastic valence force field (VFF) for (i) interpolation of impurity data for $a=\bar{a}(\frac{1}{2})$ to the alloy range ("alloy limit"), and (ii) direct optimization (u,a,c) of the CuAu I structure ("crystal limit"). The lattice parameters used for ZnS, ZnSe, and ZnTe are 5.409, 5.668, and 6.089 Å, respectively.

	Zn_2Se		Zn_2SeTe		Zn_2STe	
Quantity	Alloy limit	Crystal limit	Alloy limit	Crystal limit	Alloy limit	Crystal limit
a (Å)	$5.539=\bar{a}$	5.525	$5.879=\bar{a}$	5.868	$5.749=\bar{a}$	5.696
u	0.237	0.236	0.230	0.229	0.217	0.215
c/a	1.000	1.004	1.000	1.001	1.000	1.013
R_{AC} (Å)	2.358	2.351	2.481	2.472	2.385	2.365
R_{BC} (Å)	2.441	2.442	2.614	2.616	2.604	2.600
$\Delta E^{(2)}$ (meV/pair)	10.2	9.7	25.1	24.4	71.7	67.4

$$\mathbf{a}_1=(\tfrac{1}{2},-\tfrac{1}{2},0)a\ ,$$
$$\mathbf{a}_2=(\tfrac{1}{2},\tfrac{1}{2},0)a\ , \tag{24}$$
$$\mathbf{a}_3=(0,0,1)\eta a\ ,$$

and the atomic positions

$$\tau_A=(0,0,0)a\ ,$$
$$\tau_B=(\tfrac{1}{2},0,\eta/2)a\ ,$$
$$\tau_{C1}=(\tfrac{1}{4},\tfrac{1}{4},\eta u)a\ , \tag{25}$$
$$\tau_{C2}=(\tfrac{3}{4},\tfrac{1}{4},\eta(1-u))a\ .$$

Here, $\eta=c/a$ is the tetragonal ratio and u is the internal structure parameter ("cation displacement"). The two fundamental bond lengths in this structure,

$$R_{AC}(a,u,\eta)=[\tfrac{1}{8}+\eta^2u^2]^{1/2}a\ ,$$
$$R_{BC}(a,u,\eta)=[\tfrac{1}{8}+\eta^2(u-\tfrac{1}{2})^2]^{1/2}a\ , \tag{26}$$

are related by the cation displacement parameter

$$u=(R_{AC}^2-R_{BC}^2)/a^2\eta^2+\tfrac{1}{4}\ . \tag{27}$$

Since the binary alloys show no evidence of the existence of a unique axis we assume $c/a\equiv 1$ [in fact, optimization of the strain energy $E^{(2)}(a,c,u)$ as a function of all three parameters yields at equilibrium $c/a=1.00\pm0.01$]. The structural parameters of Eqs. (21b) are obtained by a minimization of the deformation energy in a valence-force-field (VFF) model.[62] It has been demonstrated previously[48(a),62] that whereas the *value* of the total energy of $A_nB_mC_{n+m}$ at equilibrium depends both on the (strain) deformation energy (included in our VFF) and on the chemical energy (not included), the *position* of the minimum (i.e., a_{eq} and u_{eq}) depends almost exclusively on the strain energy alone. Indeed, the values of u_{eq} for $AlGaAs_2$ (Ref. 58) and $InGaP_2$ [Ref. 48(a)] calculated from total energy minimization within the self-consistent pseudopotential method agree to 1% with those obtained in a VFF model. We use the interpolated values of $u_{eq}^{(2)}$ obtained from a valence-force-field calculation[62] for the limits $\underline{A}C:B$ and $\underline{B}C:A$. The corresponding $u_{eq}^{(2)}$ values are given in Table III in the column labeled "alloy limit," and are seen to deviate considerably from the equal bond condition ($u=\frac{1}{4}$). Alternatively, one can calculate $\{u_{eq}^{(2)},a_{eq}^{(2)},c_{eq}^{(2)}\}$ in an *ordered* CuAu I-like ABC_2 crystal by directly optimizing the total bond stretching and bond bending deformation energy. The results corresponding to this procedure are also given in Table III and denoted as "crystal limit."

Table III illustrates a number of points. *First,* the bond lengths obtained by extrapolating those pertinent to the impurity limits $\underline{A}C:B$ and $\underline{B}C:A$ (alloy limit) are close to those obtained by a full structural optimization of the ABC_2 crystal (crystal limit). The small differences that exist confirm previous results[48(a)] which indicated that the bond lengths in *ordered crystals* are somewhat closer to the ideal bond lengths $R_{\alpha\beta}^0=(\sqrt{3}/4)a_{\alpha\beta}$ than are the bonds in *disordered* or *impurity* systems [see Fig. 1 in Ref. 48(a)]. *Second,* since bond lengths in ordered systems are closer to ideality, the energy of ordered systems is lower than that of disordered systems as indicated in Sec. I A. This is illustrated in the last line of Table III, giving the deformation energy $\Delta E^{(2)}$ [i.e., the elastic piece of the formation enthalpy of the $n=2$ ordered structure]. The large elastic strain energies in $ZnSe_xTe_{1-x}$, and more so in ZnS_xTe_{1-x} are expected to lead to significant clustering (nonrandomness) in these alloys. *Third,* the tetragonal ratio c/a at equilibrium is invariably close to 1.0, i.e., tetragonal distortions are minimized. *Fourth,* variations of u (and to a lesser extent c/a) lead to bond lengths which differ considerably from those implied by VCA [i.e., $(\sqrt{3}/4)a(\frac{1}{2})$]. For example, the VCA bond length R_{Zn-S} is 2.40 and 2.49 Å in Zn_2SSe and Zn_2STe, respectively, whereas in our optimized system it is 2.36 and 2.38 Å, respectively, considerably closer to the ideal value (2.34 Å) in pure ZnS. Hence, the VCA geometry corresponds to a nonequilibrium system with exceedingly large deformation energies $\Delta E^{(2)}$. Finally, comparison of the equilibrium lattice constant obtained from full optimization to its Végard value $\bar{a}=a(\frac{1}{2})$ indicates a small downward bowing [i.e., k in Eq. (1b) is negative], e.g., deviations of -0.014, -0.011, and -0.033 Å for Zn_2SSe, Zn_2SeTe, and Zn_2STe, respectively, at $x=\frac{1}{2}$.

TABLE IV. Character table for D_{2d}.

D_{2d}		E	C_2	$JC_4(2)$	$C_2(2)$	$JC_2(2)$
Γ_1	M_1	1	1	1	1	1
Γ_2	M_2	1	1	−1	1	−1
Γ_3	M_3	1	1	1	−1	−1
Γ_4	M_4	1	1	−1	−1	1
Γ_5	M_5	2	−2	0	0	0

Our calculated bond lengths R_{AC} and R_{BC} of Table III agree remarkably well with recent EXAFS measurements[87] on $ZnSe_xTe_{1-x}$ alloys: These experiments[87] yield, for $x=\frac{1}{2}$, $R_{Zn-Se}=2.472$ Å (calculated value in Table III: 2.472 Å) and $R_{Zn-Te}=2.617$ Å (calculated value in Table III: 2.616 Å). This excellent agreement obtained for bond lengths (hence for the anion displacement parameter u) lends support to our structural model. (The formation enthalpies of $n=2$ *ordered* alloys, of which $\Delta E^{(2)}$ in Table III represents the elastic piece, have not been measured experimentally.)

C. Folding of bands and interacting bands

The choice of the CuAu I structural model removes some of the constraints previously imposed on alloy calculations within the VCA (Sec. I B). First, since in the CuAu I structure each Zn atom is surrounded by two different pairs of anions (e.g., S and Se), the top of the valence band is no longer restricted to be non-s-like (as in the zinc-blende case), hence bowing of the spin-orbit splitting is allowed. Second, coupling between certain zinc-blende bands is permitted, since each **k** vector in the CuAu I structure is describable by a (superlattice-like) folding of the **k** vectors of the zinc-blende lattice [see Eq. (28) below]. Third, the existence of an internal structural parameter [u of Eq. (27)] makes it possible to assign different lengths to the two bonds R_{AC} and R_{BC}, without violating Végard's rule for the lattice constant. Fourth, no averaging of the potentials of the alloyed sublattices is necessary, hence charge redistribution between them can be described self-consistently.

It is useful to compare the band structure of ABC_2 to those of its parent compounds AC and BC in steps. First, suppose we neglect any non-zinc-blende component in the crystal potential of the ABC_2 system and assume $c/a=1$ and $u=\frac{1}{4}$. At this limit the bands of ABC_2 can be obtained by folding the zinc-blende (ZB) bands into the tetragonal Brillouin zone. Each **k** vector (a,b,c) in the tetragonal zone then corresponds to two

TABLE V. Character table for C_{2v}.

C_{2v}	E	C_2	JC_2	JC_2
R_1	1	1	1	1
R_2	1	−1	−1	1
R_3	1	1	−1	−1
R_4	1	−1	1	−1

TABLE VI. Character table for C_2.

C_2	E	C_2
Σ_1	1	1
Σ_2	1	−1

ZB **k** vectors (a,b,c) and $(a,b,c\pm1)$. At high-symmetry points we have the correspondence relations (denoting states of ABC_2 by a bar)

$$\begin{aligned}
&\bar{\Gamma}\leftrightarrow\Gamma+X_z\ ,\\
&\bar{M}\leftrightarrow X_x+X_y\ ,\\
&\bar{R}\leftrightarrow L+L\ ,\\
&\bar{A}\leftrightarrow W+W\ ,
\end{aligned}\tag{28}$$

etc., where the x, y, and z directions are parallel to the a, b, and c axes of the crystal, respectively. Placing the origin of the coordinate system on the anion, the mapping for common-cation ABC_2 systems gives $X_1\leftrightarrow\bar{\Gamma}_1+\bar{M}_1+\bar{M}_2$ and $X_3\leftrightarrow\bar{\Gamma}_4+\bar{\Gamma}_5$. (The converse is true for common-anion systems: $X_3\leftrightarrow\bar{\Gamma}_1+\bar{M}_1+\bar{M}_2$ and $X_1\leftrightarrow\bar{\Gamma}_4+\bar{\Gamma}_5$). This mapping could create extra degeneracies at points such as $\bar{M}$ and $\bar{R}$, where the states result from folding of two zinc-blende bands at equivalent k points. Note that this folding introduces "pseudodirect" states, e.g., at the $\bar{\Gamma}$ point in the conduction band one will find both $\bar{\Gamma}_{1c}(\Gamma_{1c})$ and $\bar{\Gamma}_{1c}(X_{1c})$; had $\bar{\Gamma}_{1c}(X_{1c})$ been the lowest, the band gap would be "pseudodirect."[56,57] Second, introduce the perturbation $\Delta V(\mathbf{r})=V_{tet}(\mathbf{r})-V_{ZB}(\mathbf{r})$. This perturbation has three components: (i) the contribution due to $A\neq B$, (ii) that due to $u\neq\frac{1}{4}$, and (iii) the effect of $c/a\neq1$. Any of these interactions can lift degeneracies present following the first step (e.g., the $\bar{\Gamma}_4$ and $\bar{\Gamma}_5$ states at the valence-band maximum Γ_{15} become nondegenerate; the same is true for $\bar{M}_1$ and $\bar{M}_2$ evolving from X_1). In the usual VCA band structure of an alloy both folding (first step) and coupling (second step) effects are missing (although, clearly the disparity between *different* VCA-ZB states, such as Γ_1 and X_1, still exists). One expects that disorder effects will broaden somewhat the folded and interaction-split bands calculated here; however, in the cases where large splittings are predicted for the ordered systems, we expect them to survive disorder broadening and hence be observed experimentally even in disordered samples. Similar considerations apply for folding of the ZB or CuAu I states into Cu_3Au states. Denoting the Γ state of Cu_3Au by $\hat{\Gamma}$, we have

$$\begin{aligned}
&\hat{\Gamma}\leftrightarrow\Gamma+X_x+X_y+X_z\quad(Cu_3Au\text{–zinc-blende})\ ,\\
&\hat{\Gamma}\leftrightarrow\bar{\Gamma}+\bar{M}\quad(Cu_3Au\text{–CuAu I})\ .
\end{aligned}\tag{29}$$

Further discussion of the symmetry and folding effects can be found in Ref. 88(a). The notation for the symmetry labels used for the CuAu I–like structures is defined in Tables IV–VI. The labels used for the zinc-blend structure follow the convention of Parmenter.[88(b)]

TABLE VII. Calculated (in eV) band eigenvalues at high symmetry points in the zinc-blende Brillouin zone of binary zinc chalcogenides, relative to the valence-band maximum. PVMB, potential variation mixed basis (present calculation); FLAPW, full linear augmented plane wave; LCGO, linear combination of Gauss orbitals; SCOPW, self-consistent orthogonalized plane waves; KKR, Korringa-Kohn-Rostocker; EM-NLP, empirical nonlocal pseudopotential. The symbols CA, W, W-SR, and $\alpha=1$ refer to the type of exchange correlation used, i.e., Ceperley-Alder, Wigner, semirelativistic Wigner, and Slater, respectively.

State	ZnS PVMB CA $a=5.409$ Å	ZnSe PVMB CA $a=5.668$ Å	ZnTe PVMB CA $a=6.089$ Å	ZnTe PVMB W $a=6.089$ Å	ZnTe[a] FLAPW W $a=6.089$ Å	ZnTe[a] FLAPW W-SR $a=6.089$ Å	ZnS[b] LCGO W $a=5.409$ Å	ZnSe[b] LCGO W $a=5.668$ Å	ZnS[c] SCOPW $\alpha=1$ $a=5.41$ Å	ZnSe[c] SCOPW $\alpha=1$ $a=5.65$ Å	ZnS[d] KKR $\alpha=1$ $a=5.41$ Å	ZnSe[e] EM-NLP $a=5.65$ Å
Γ_{1v}	−13.06	−12.86	−11.16	−11.18	−11.06	−11.93	−12.89	−12.67	−11.77	−11.82		−12.25
$\Gamma_{15v}(d)$	−7.65	−7.86	−8.26	−7.84	−7.56	−7.27	−6.4	−6.7	−14.1	−12.6		
$\Gamma_{12v}(d)$	−7.27	−7.50	−8.13	−7.66	−7.36	−7.05	−6.4	−6.7				
Γ_{15v}	0.00	0.00	0.00	0.00	0.00	0.00	0.00	0.00	0.00	0.00	0.00	0.00
Γ_{1c}	1.96	1.45	1.89	1.82	2.01	0.96	2.26	1.83	3.77	2.94	3.7	2.76
Γ_{15c}	6.45	5.77	4.21	4.16	4.15	4.23	7.04	5.86	7.99	6.66	9.0	~7.37
Γ_{1c}	11.59	9.79	7.10	6.99	7.05	6.89						
X_{1v}	−11.88	−11.79	−9.97	−9.90	−9.71	−10.72	−11.67	−11.55	−10.29	−10.48		−10.72
X_{3v}	−7.61	−4.82	−5.14	−5.16	−5.10	−5.18	−4.49	−4.69	−3.93	−4.31		−4.96
X_{5v}	−2.30	−2.20	−2.27	−2.30	−2.26	−2.25	−2.19	−2.16	−1.61	−1.65	−1.4	~−2.06
X_{1c}	3.18	2.88	2.23	2.17	2.20	2.13	3.61	3.18	5.01	4.19	5.8	~−4.86
X_{3c}	4.08	3.47	2.12	2.07	2.08	2.05	4.58	3.64	5.95	4.49	6.1	
X_{1c}	10.70	10.58	10.10	10.00			10.92	10.85				
L_{1v}	−12.17	−12.06	−10.25	−10.22	−10.16	−11.04	−11.97	−11.83	−10.66	−10.84		−11.08
L_{1v}	−5.38	−5.21	−5.27	−5.33	−5.25	−5.33	−5.20	−5.15	−4.20	−4.40		−5.08
L_{3v}	−0.94	−0.87	−0.94	−0.96	−0.94	−0.94	−0.84	−0.85	−0.61	−0.64	−0.6	~−0.9
L_{1c}	3.24	2.63	1.96	1.90	1.99		3.65	2.91	4.96	3.79	5.3	3.96
L_{3c}	6.96	6.36	4.87	4.82	4.82		7.51	6.70	8.62	7.31	9.3	~7.7

[a]Self-consistent FLAPW calculation of Wei and Zunger using ~200 basis orbitals/cell and two **k** points (Ref. 89).

[b]Self-consistent LCGO calculation of Wang and Klein using a basis of 45 and 54 Gauss orbitals/cell for ZnS and ZnSe, respectively, and 10 special **k** points, Ref. 90.

[c]Self-consistent OPW model of Stukel *et al.* using 229 OPW/cell and iterating over four (high-symmetry) **k** points, Ref. 91; see also Ref. 92.

[d]Non-self-consistent KKR model of Eckelt *et al.* using an adjustable muffin-tin potential (Ref. 93).

[e]Non-self-consistent pseudopotential model of Chelikowsky and Cohen fit to the then-available experimental data, using a plane-wave basis of 50 functions/cell, Ref. 94. See also Refs. 95–97.

IV. ELECTRONIC STRUCTURE OF ZnS, ZnSe, AND ZnTe

A. Band structures

Figure 2 depicts the self-consistent nonrelativistic band structures of ZnS, ZnSe, and ZnTe at their experimental lattice constants (Table III), calculated with the Ceperley-Alder exchange correlation. Table VII[89–97] gives band eigenvalues at high symmetry points in the Brillouin zone. (Our results for ZnS differ from our previously published results[82] which used the Wigner correlation only due to the different choice of exchange correlation.) The results for ZnS and ZnSe are similar to those obtained by Wang and Klein[90] (using the Wigner correlation), although some differences exist (interpreted in Ref. 82 to arise from insufficient convergence of the basis set used by Wang and Klein). The present results for ZnTe agree well with the results obtained by the full

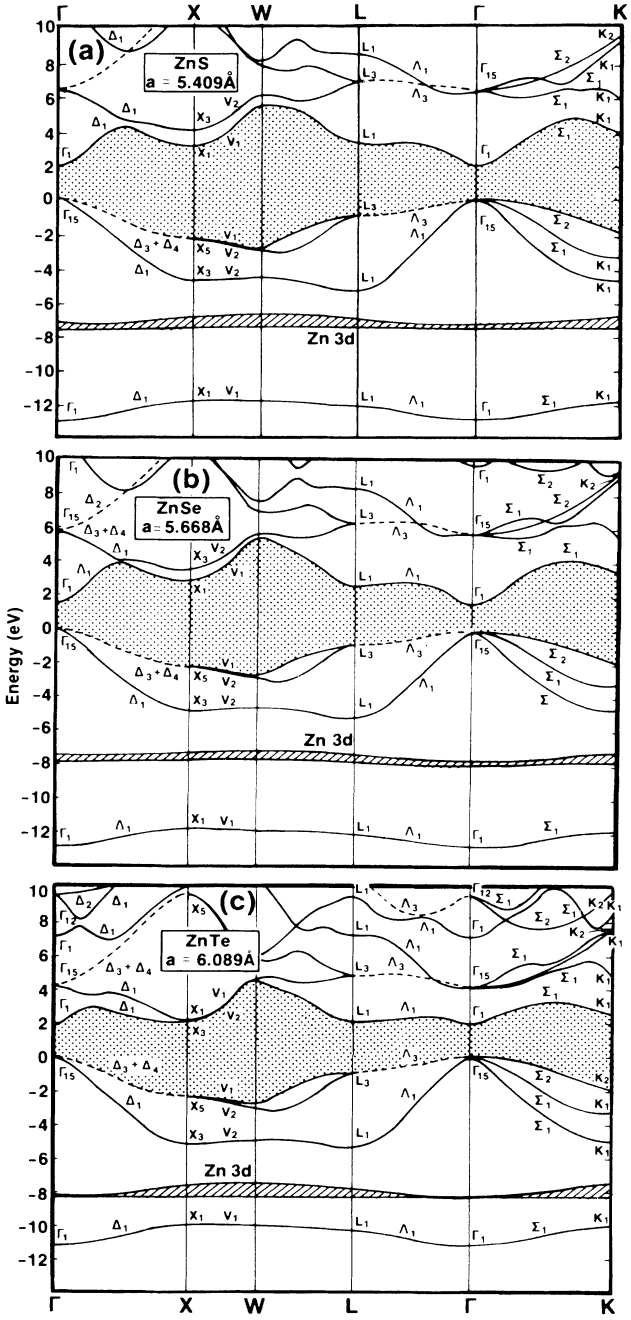

FIG. 2. Nonrelativistic self-consistent local-density band structures of (a) ZnS, (b) ZnSe, and (c) ZnTe calculated with the Ceperley-Alder exchange correlation. Dashed lines show doubly degenerate bands; shaded areas denote the fundamental band-gap regions. The origin of the coordinate system is on the anion site. Results are also summarized in Table VII for high-symmetry points. All gaps are direct.

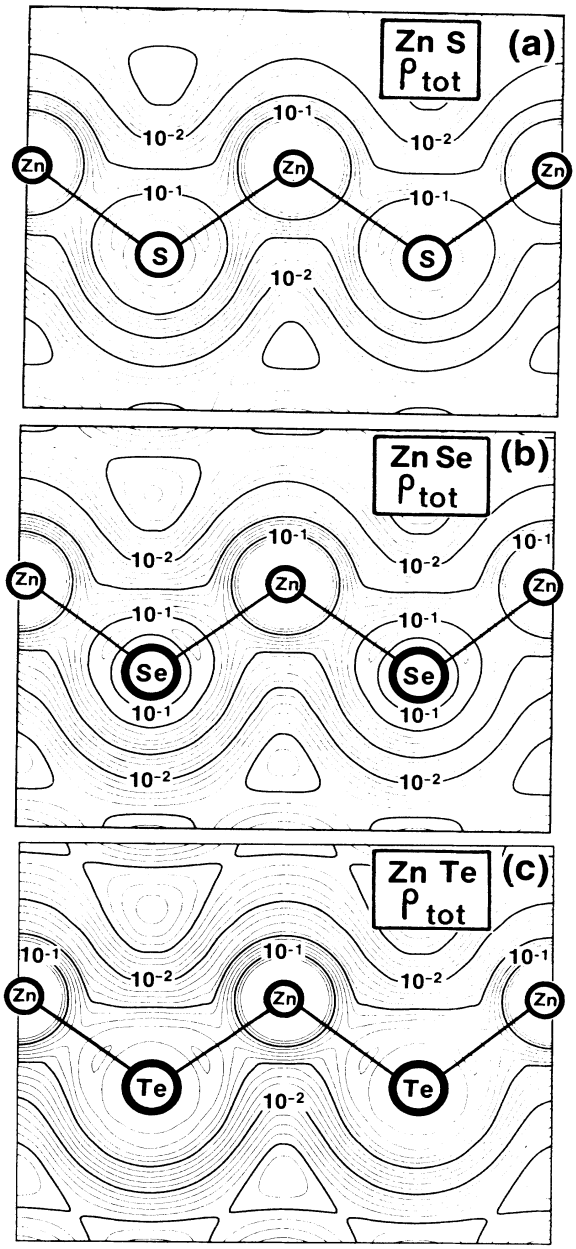

FIG. 3. Logarithmically spaced charge-density contours for the valence bands of (a) ZnS, (b) ZnSe, and (c) ZnTe in the (110) plane, given in units of e/a.u.^{3}. The solid circles represent the core regions inside which the high charge density is truncated for clarity of display.

TABLE VIII. Observed and calculated interband transition energies (in eV) for cubic ZnS, ZnSe, and ZnTe.

Transition or energy separation	ZnS		ZnSe		ZnTe	
	Expt.	Calc.	Expt.	Calc.	Expt.	Calc.
Photoemission						
$\Gamma_{1v} \rightarrow \Gamma_{15v}$	-13.5[a]	-13.06	15.2 ± 0.6	-12.86	-13.0[a]	-11.16
$X_{1v} \rightarrow \Gamma_{15v}$	-12.0[a]	-11.88	-12.5 ± 0.4[a]	-11.79	-11.6[a]	-9.97
$L_{1v} \rightarrow \Gamma_{15v}$	-12.4[a]	-12.17	-13.1[a]	-12.06	-12.0[a]	-10.25
$\Gamma(d) \rightarrow \Gamma_{15v}$	-10.11[a]	~ -7.4	-10.33[a]	~ -7.6	-10.01[a]	~ -8.1
$X_{3v} \rightarrow \Gamma_{15v}$	-5.5[a]	-4.80	-5.3 ± 0.3[b]	-4.82	-5.5[a]	-5.14
$X_{5v} \rightarrow \Gamma_{15v}$	-2.5[a]	-2.30	-2.1 ± 0.3	-2.20	-2.4[a]	-2.27
$L_{3v} \rightarrow \Gamma_{15v}$	-1.4[a]	-0.94	-1.3 ± 0.3[a]	-0.87	-1.1[a]	-0.94
Reflectivity						
$L_{3v} \rightarrow L_{1c}$	5.81[c]	4.17	4.91[c]	3.50	3.45[d,e]	2.89
$\Gamma_{15v} \rightarrow \Gamma_{15c}$	8.35[f]	6.45	7.80[d]	5.77	4.82[e]	4.21
$\Gamma_{15v} \rightarrow \Gamma_{1c}$	3.80[c]	1.96	2.82[c]	1.45	2.39[g]	1.89
$X_{5v} \rightarrow X_{1c}$	6.6[c]	5.48	6.00[h]	5.08	5.45[e]	4.49

[a]Reference 98.
[b]Reference 99.
[c]Reference 100.
[d]Reference 97.
[e]Reference 101.
[f]Reference 102.
[g]Reference 103.
[h]Reference 104.

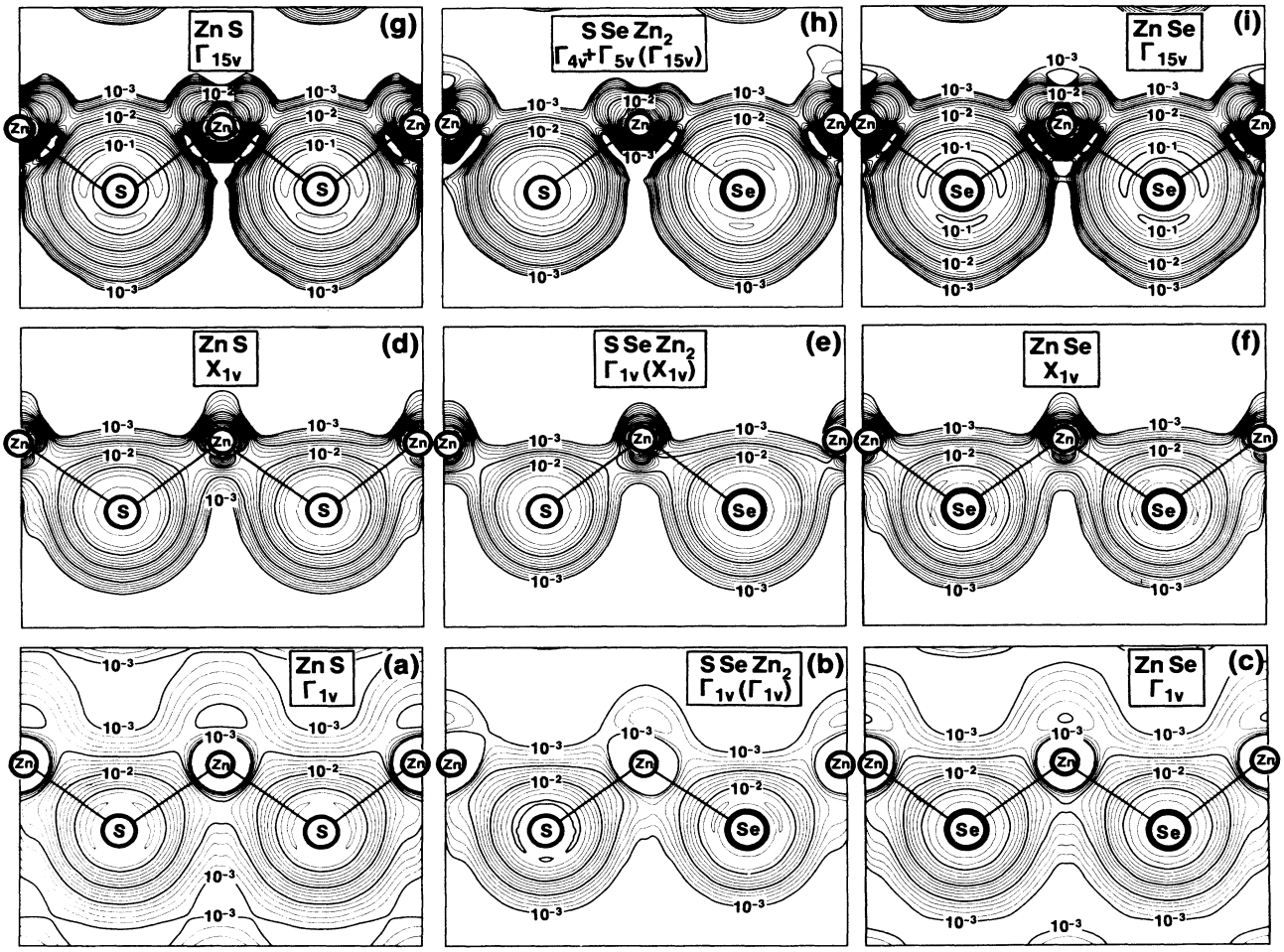

FIG. 4. Electronic charge density in the (110) plane (logarithmically spaced contours, in units of e/a.u.^{3}) of high symmetry *valence*-band states in ZnS (left), ZnSe (right), and the corresponding states in relaxed $SSeZn_2$ (center).

linear augmented-plane-wave (FLAPW) method[89] (Table VII), using the same exchange-correlation functional (columns 5 and 6 in Table VII). The largest difference is in the position of the Zn $3d$ bands (0.3 eV deeper in the present calculation). Our results show significant differences relative to older (non-self-consistent) orthogonalized plane-wave (OPW) calculations of Herman *et al.*[92] and the Korringa-Kohn-Rostoker (KKR) results of Eckelt *et al.*,[93] as well as with respect to the empirically adjusted pseudopotential calculations.[94–97] They are more similar to the results of the self-consistent OPW calculation of Stukel *et al.*[91] Comparison of the calculated and observed interband transition[97–104] energies (Table VIII) shows the expected[86] underestimation of the local-density model. In particular, ionization of an electron from the d band (e.g., in a photoemission experiment) is expected to lead to a downward relaxation relative to the band model results.

B. Effect of cation d states on the fundamental band gaps in II-VI compounds

In comparing the direct $\Gamma_{15v} \rightarrow \Gamma_{1c}$ band gaps ε_g in a sequence of materials which do not have a d state inside the valence band one notices a gradual decrease as the anion becomes heavier, e.g., GaP (2.4 eV)→GaAs (1.5 eV)→GaSb (0.81 eV), or InP (1.42 eV)→InAs (0.43 eV)→InSb (0.24 eV). This was traditionally explained[105] in terms of the decrease in the p orbital ionization energies of the anion in this series (i.e., P→As→Sb). In contrast, when a chemically active d band exists inside the valence band (II-IV compounds, see Fig. 2) there is an additional contribution[57] to the band gap, which was not recognized by simple s-p orbital models (both tight-binding[66,105] and pseudopotential[94–97]): The cation d orbital transforms in the T_d site symmetry as $\Gamma_{15}(d)+\Gamma_{12}(d)$ having hence a common representation with the anion p orbitals [transforming as $\Gamma_{15}(p)$]. These $\Gamma_{15}(p)$ and $\Gamma_{15}(d)$ unperturbed zero-order states can therefore interact, forming a bonding-antibonding pair, the latter being the valence-band maximum (VBM) at Γ. This interaction hence repels the VBM upwards by $\sim |\langle \Gamma_{15}(d) | V | \Gamma_{15}(p) \rangle|^2/(\varepsilon_d - \varepsilon_p)$, reducing thereby the band gap relative to analogous systems with no active d electrons (e.g., III-V compounds). This reduction in the band gap becomes pronounced when the energy denominator $\varepsilon_d - \varepsilon_p$ becomes small. Since the

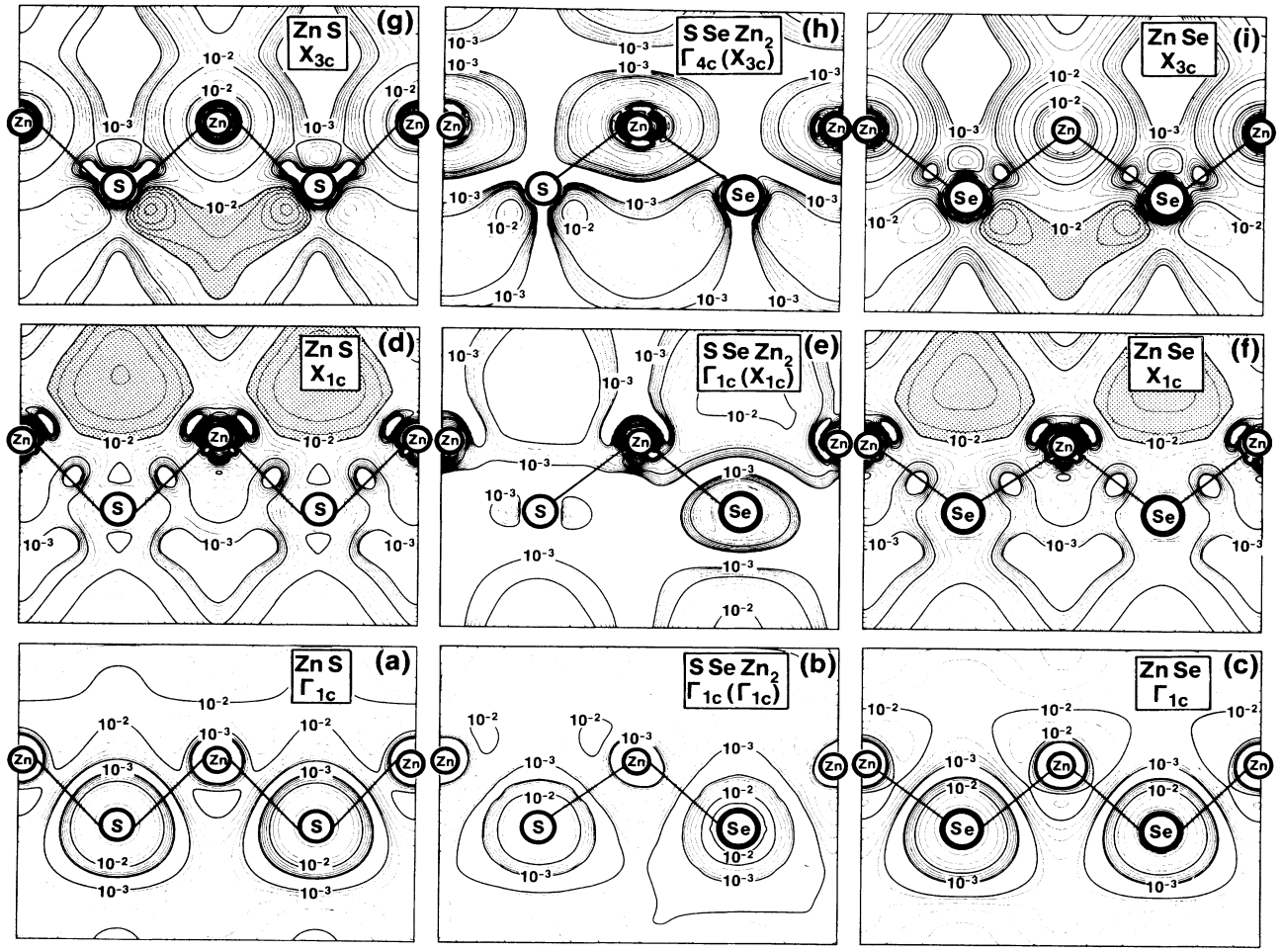

FIG. 5. Same as Fig. 4, but for *conduction* bands. The shaded regions highlight the interstitial space with large electron-density amplitudes.

sulfur p orbital is far deeper (i.e., has a higher ionization potential) than the Se p or Te p orbitals, the band-gap reduction is strongest for ZnS, and weaker in ZnTe. In Ga or In containing III-V materials the cation $3d$ orbital is deep enough ($\sim E_v - 18$ eV) to make these effects small (although non-negligible on the scale of the smaller gaps of III-V systems). Calculations based on s-p orbitals only[66,94–97,105] miss this effect, producing spuriously large band gaps for II-VI's (unless the empirical band-structure parameters are readjusted). Such is the case in Harrison's tight-binding model[105] which overestimates the $\Gamma_{15v} \rightarrow \Gamma_{1c}$ band gap by a factor of 3 (see Fig. 6.8 in Ref. 105). This effect is naturally smaller in Cd chalcogenides since the Cd $4d$ orbital is deeper than the Zn $3d$ orbital. This p-d repulsion mechanism was previously used[57] to explain the anomalously small band gaps in copper chalcogenides $CuB^{III}S_2$, $CuB^{III}Se_2$, and $CuB^{III}Te_2$ (where B^{III}=Al,Ga,In) relative to the analogous zinc chalcogenides ZnS, ZnSe, and ZnTe. This explains also why the decrease in the band gaps in going from $A^{II}Se$ to $A^{II}Te$ (A^{II}=Zn,Cd,Hg) is far smaller than in going from $B^{III}As$ to $B^{III}Sb$ [e.g., the direct band gaps are ZnSe (2.8 eV)→ZnTe (2.4 eV); CdSe (1.85 eV)→CdTe (1.60 eV); HgSe (−0.2 eV)→HgTe (−0.3 eV) compared with the far larger change in GaAs (1.5 eV)→GaSb (0.8 eV)].

The substantial effect of the cation d orbitals on the *charge densities* of II-VI materials is discussed in Sec. IV D.

C. Relativistic effects

Relativistic effects can change the *trends* in the band gaps in the ZnS→ZnSe→ZnTe series. In a *nonrelativistic* calculation (columns 2, 3, and 4 in Table VII) we find the direct band gaps ZnS (1.96 eV)→ZnSe (1.45 eV) →ZnTe (1.89 eV), i.e., a nonmonotonic change between ZnSe and ZnTe (due to the relative unimportance of the p-d repulsion effect in ZnTe discussed above). However, relativistic corrections[89] (column 7 in Table VII) substantially lower the band gap of ZnTe (in proportion to ZnS and ZnSe), restoring the monotonic decrease in the band gaps in their series observed experimentally.

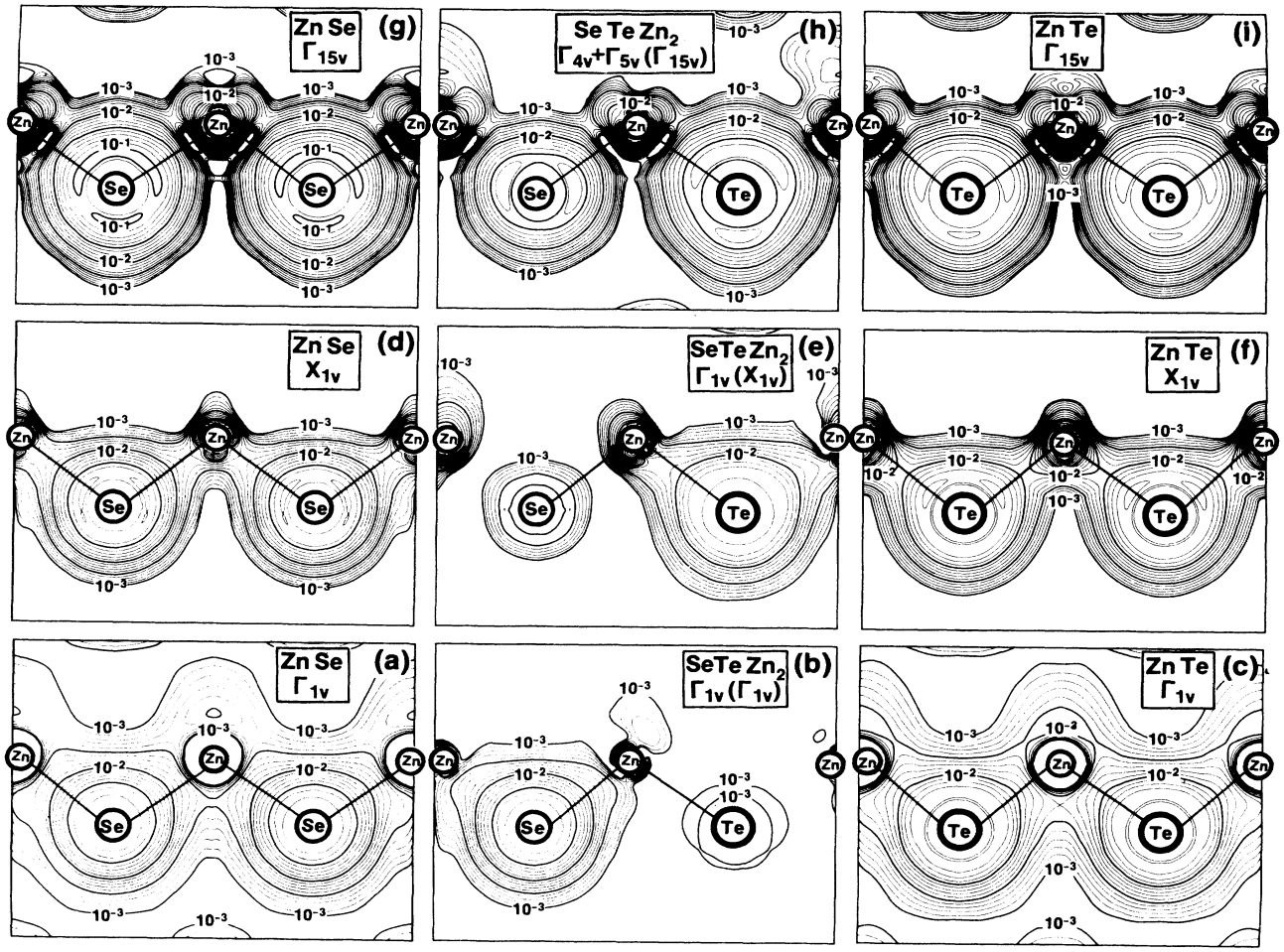

FIG. 6. Electronic charge density in the (110) plane (logarithmically spaced contours in units e/a.u.^{3}) of high-symmetry *valence*-band states in ZnSe (left), ZnTe (right), and the corresponding states in relaxed $SeTeZn_2$ (center).

D. Charge densities

1. Total valence densities

Figure 3 depicts the calculated valence charge densities of ZnS, ZnSe, and ZnTe in the (110) plane of the zinc-blende lattice. The results for ZnSe are similar to those obtained by Wang and Klein[90] in their self-consistent linear combination of Gaussian orbitals (LCGO) calculation. The results differ considerably, however, from those obtained in empirical pseudopotential models.[94–96] In particular, since the Zn d potentials (hence bands) are missing in most plane-wave pseudopotential studies, these models have consistently underestimated the *cation* character of the Γ_{15} valence-band maximum [compare Fig. 3 here with Fig. 2 of Ref. 96(a) and Fig. 18 of Ref. 96(c)].

2. Band-by-band charge densities

It is interesting to consider the resolution of the total valence-band charge densities of Fig. 3 into their band-by-band components (Figs. 4–9). The bottom of the valence band occurs at the Γ_{1v} point. This state is composed primarily of anion s orbitals, as can be seen from the charge densities depicted in Fig. 4(a) (for ZnS), Fig. 4(c) (for ZnSe), and Fig. 6(c) (for ZnTe), exhibiting a gradual delocalization, characteristic of the orbital expansion in the S $3s \rightarrow$Se $4s \rightarrow$Te $5s$ sequence. The conduction-band state Γ_{1c} is complementary to Γ_{1v} in being its antibonding counterpart: Its charge density for ZnS [Fig. 5(a)], ZnSe [Fig. 5(c)], and ZnTe [Fig. 7(c)] exhibits a node along the anion-cation bond direction. However, whereas the bonding Γ_{1v} has most of its contribution from *anion* s orbitals, the antibonding Γ_{1c} has also a sizeable contribution from the *cation* s orbitals. Note that the Γ_{1c} state is highly localized around the anions and cannot be thought of as a "nearly free electron" band, as are higher-energy conduction bands.

The valence-band state X_{1v} is seen to be an anion s state (with some cation p character) in ZnS [Fig. 4(d)], ZnSe [Fig. 4(f)], and ZnTe [Fig. 6(f)]. Its antibonding counterpart is the conduction-band state X_{1c} shown for

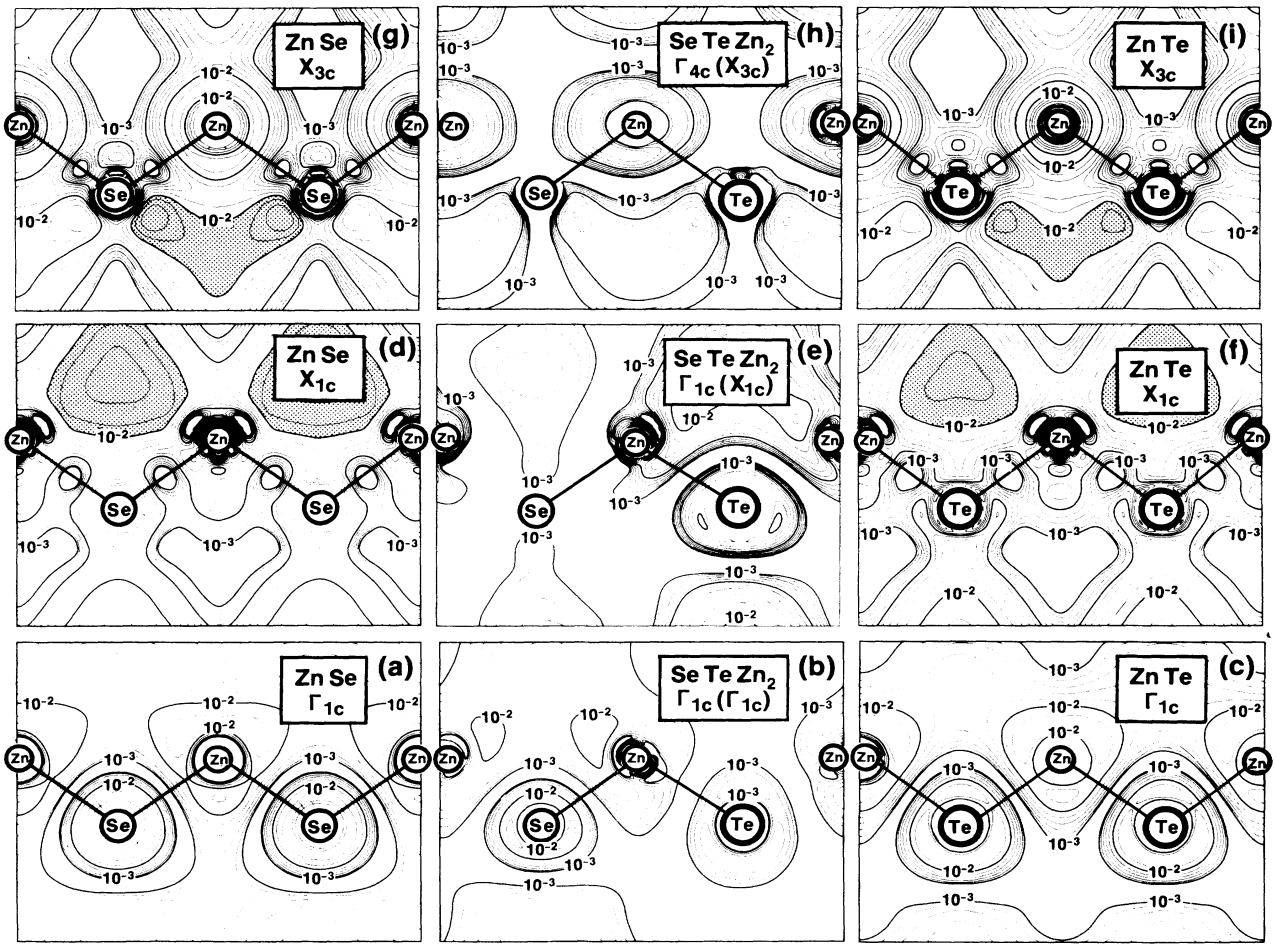

FIG. 7. Same as Fig. 4, but for *conduction* bands. The shaded regions highlight the interstitial space with large electron-density amplitudes.

ZnS [Fig. 5(d)], ZnSe [Fig. 5(f)], and ZnTe [Fig. 7(f)] [having chosen the origin of the coordinate system to be on the anion site, the X_1 (X_3) state has *s-d* character on the anion (cation) and *p-d* character on the cation (anion)]. The important distinction between the bonding-antibonding X_{1v}-X_{1c} pair is that in the X_{1v} state (much as in the Γ_{1v} state) charge is centered on *atoms,* whereas in the X_{1c} state most of the charge is *between the atoms* i.e., on the interstitial sites. We see for example that the X_{1c} state has most of its amplitude [shaded areas in Figs. 5(d), 5(f), and 7(f)] on the interstitial region *between the cations.* The conduction band X_{3c} is complementary to X_{1c} in that it has most of its amplitude in the interstitial volume *between the anions* [shaded areas in Figs. 5(g), 5(f), and 7(i)]. Very little charge resides on the atomic sites in X_{1c} and X_{3c}. Simple tight-binding models[105] that use a minimal basis set and confine these basis functions to *atomic* sites cannot[106] properly describe the charge distribution of X_{1c} or X_{3c} (although empirical parametrization of the Hamiltonian can be used to fix the band energies). [Note that having chosen the origin of our coordinate system at the anion site, Eq. (25), we find the X_{1c} state in ZnS and ZnSe to be lower in energy than the X_{3c}, hence X_{1c} and X_{3c} interchange their roles relative to Ref. 106, where the origin was chosen to be on the cation site.]

The top of the valence band occurring at the Γ_{15v} state is seen in Fig. 4(g) (ZnS), Fig. 4(i) (ZnSe), and Fig. 6(i) (ZnTe) to be formed of anion *p* orbitals *and* Zn 3*d orbitals.* The direct $\Gamma_{15v} \rightarrow \Gamma_{1c}$ transition hence couples initial and final states with amplitude *on the same (anion) sublattice.* In contrast, simple tight-binding models[105] which describe the conduction band minimum Γ_{1c} primarily as a *cation*-like state suggest the $\Gamma_{15v} \rightarrow \Gamma_{1c}$ direct transition to couple the anion sublattice (Γ_{15v}) with the cation sublattice (Γ_{1c}), i.e., to be a two-center excitation. While this is a valid description in the extreme ionic limit (e.g., NaCl, where Γ_{1c} is indeed a cation state), we see that this is an incorrect description in the semiconducting limit, even for the relatively ionic zinc chalcogenides.

E. Effect of cation *d* states

Recently, Wentzcovitch *et al.*[94(b)] have performed an empirical nonlocal pseudopotential calculation for ZnSe and displayed the calculated band-by-band charge densities. Their results are generally similar to ours; however, since they omitted the Zn *d* pseudopotential in their cal-

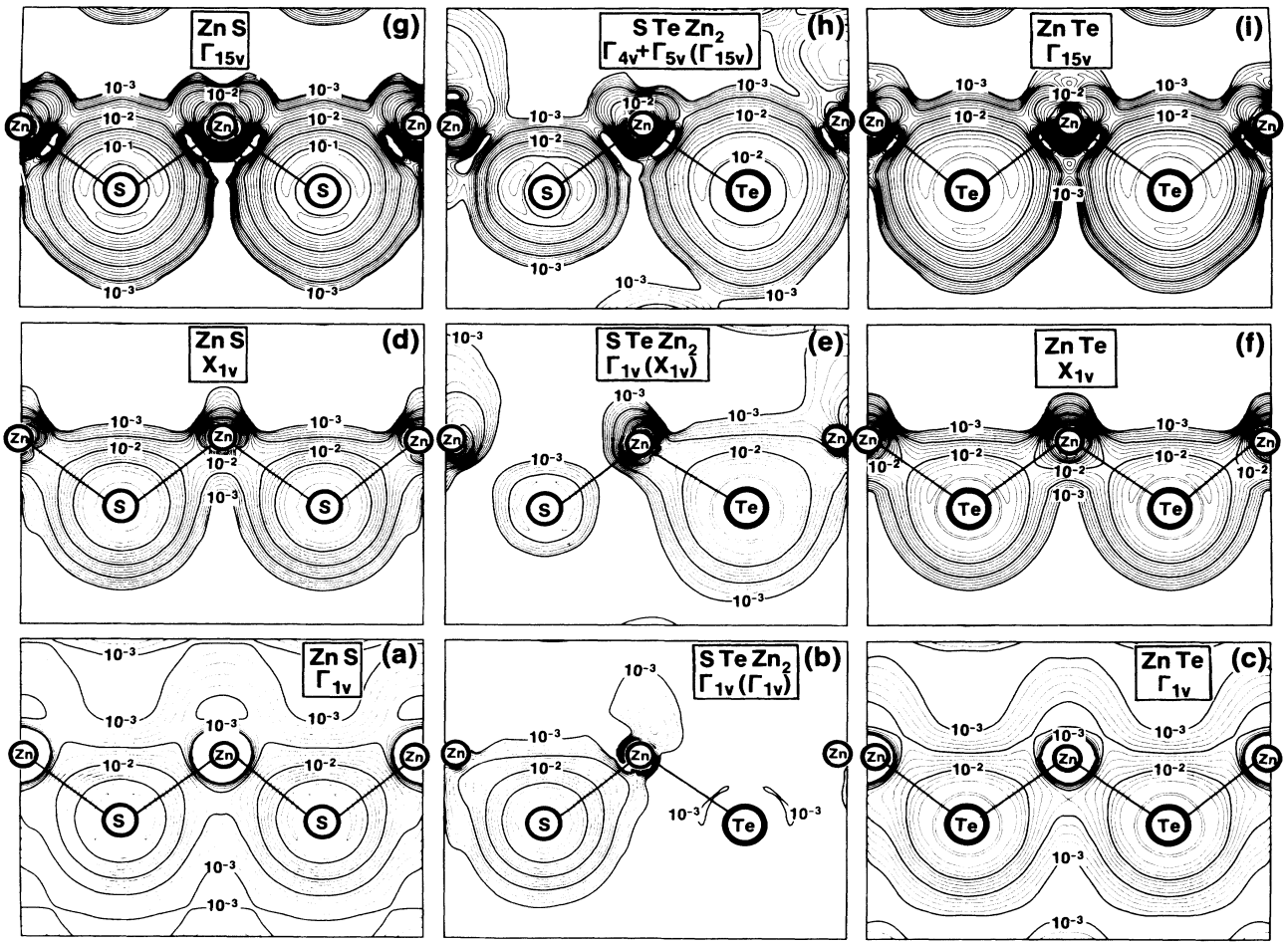

FIG. 8. Electron charge-density in the (110) plane (logarithmically spaced contours, in units of e/a.u.^{3}) of high-symmetry *valence*-band states in ZnS (left), ZnTe (right), and the corresponding states in relaxed $STeZn_2$ (center).

culation, the *p-d* repulsion effect present in our work (see Sec. IV A) is missing. This results in a spurious enhancement of anion and cation *p* character relative to cation *d* character in states such as the VBM [compare their Fig. 1(a) with our 4(i)], and in a displacement of cation *d* character in favor of cation *p* character in states such as the X_{1c} [compare their Fig. 3(c) with our 5(f)].

The ability of empirical pseudopotential[94–97] and tight-binding[66,105] methods to reproduce the global features of the electronic structure of II-VI compounds without including the cation *d* band *(which is inside the valence band)* may seem paradoxical. Our analysis reveals, however, the mechanism of this success. As discussed in Sec. IV B, the omission of the cation *d* levels from the spectrum eliminates the *p-d* repulsion with the anion *p* states. All other things being equal, this would have substantially *increased* the direct band gap, (as the anion *p* band is not repelled upwards in the absence of lower *d* bands). Using, however, the adjustable parameters available in such empirical methods, it is still possible to fit the band gaps by *lowering* the conduction bands. Since the latter involve mostly *cation* states, this could be accomplished by using weaker cation potentials than would have been required in the presence of the cation *d* states. Indeed, cation atomic levels calculated from such interpolated pseudopotentials yield *s* and *p* binding energies that are 1–3 eV too *small.* However, using such spuriously weak cation potentials invariably reduces the cation content of the valence-band charge density, as observed by comparing the present all-electron charge densities with those obtained by empirical pseudopotential methods.[94–97] It hence appears that good fits to *energies,* along with some misrepresentations of *charge densities* are common features of empirical pseudopotential calculations of such systems. The evidence for the existence of significant cation character in the valence band of II-VI materials (in addition to the obvious *d* states observed in photoemission; see Table VIII) is nonetheless compelling, and includes their indirect effect on band gaps (Sec. IV B), doping behavior (Sec. IV B), the existence of substantial valence-band offsets in common-anion II-VI pairs[107–108] (e.g., CdTe-

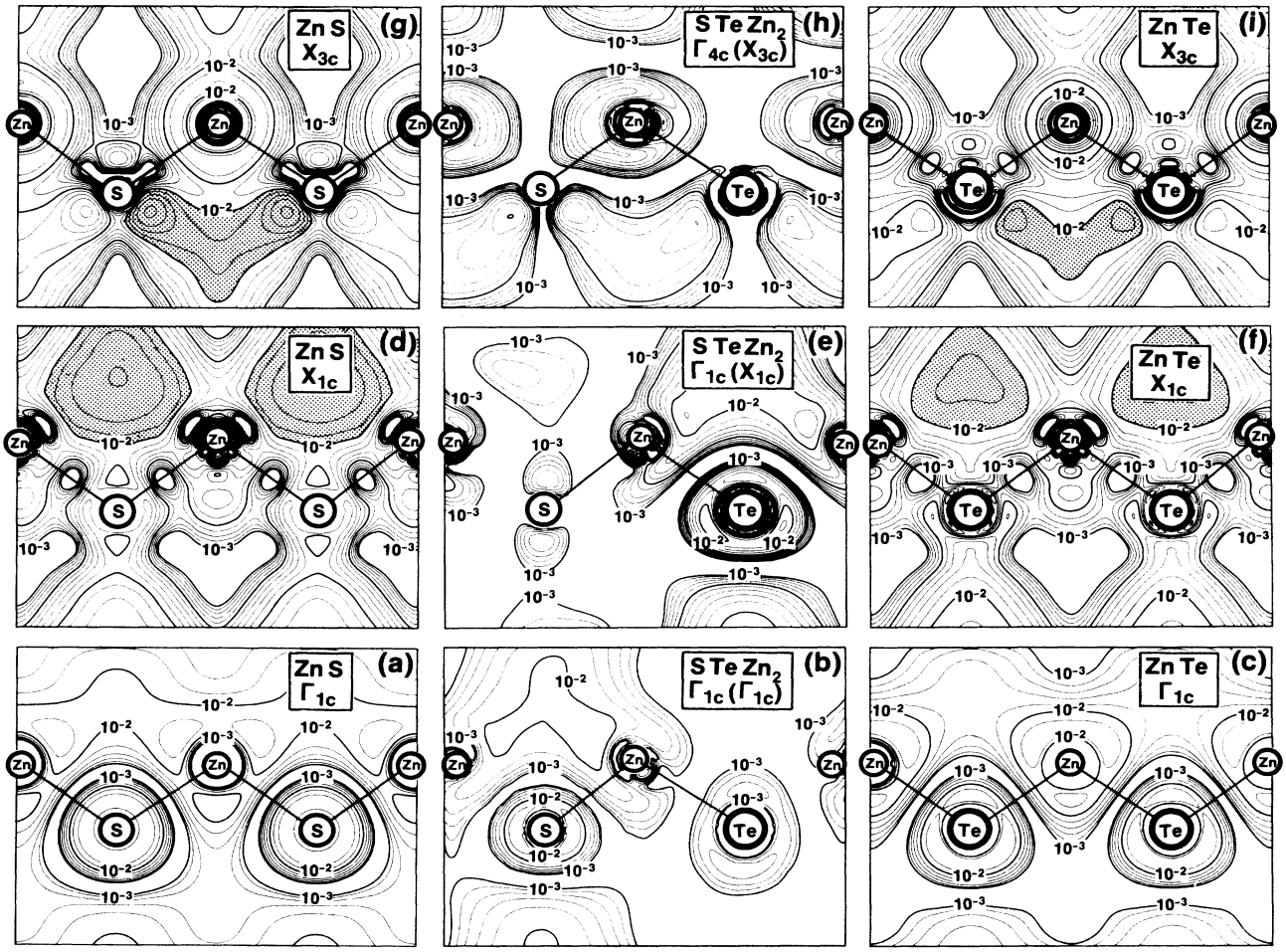

FIG. 9. Same as Fig. 8, but for *conduction* bands.

TABLE IX. Calculated electronic x-ray structure factors (in e/mol), for group-(i) reflections [Eq. (36)]. The total number of electrons per mole is denoted $\rho(\mathbf{G}=\mathbf{0})$. Origin at the anion site for the ZB structure and at the X-anion in the Zn_2XY ternary. Experimental results are given for ZnSe.

Beam	ZnS $\rho(0)=46$	ZnSe $\rho(0)=64$	ZnTe $\rho(0)=82$	ZnSe expt.[a] $\rho(0)=64$	Zn_2SSe $\rho(0)=110$	Zn_2SeTe $\rho(0)=146$	Zn_2STe $\rho(0)=128$
[111]	28.47	39.00	52.46	39.6±0.4	66.06	90.72	76.79
[200]	13.04	3.04	18.38	3.7±0.14	10.07	21.31	4.99
[002]					9.42	22.80	9.19
[220]	31.48	47.16	62.38	47.4±0.5	78.57	109.43	93.45
[202]					77.99	108.07	89.66
[311]	22.07	31.21	42.96	32.3±0.5	51.92	73.51	61.15
[113]					51.07	72.10	56.75
[222]	11.16	2.63	15.63	2.9±0.15	8.17	19.32	7.31
[400]	26.26	40.22	54.01	40.6±0.45	66.37	94.09	79.66
[004]					64.41	89.53	67.34
[331]	18.91	27.23	38.02	27.4±0.5	44.92	64.63	53.39
[313]					44.20	63.44	49.66
[420]					6.55	17.03	4.37
[402]	9.21	2.86	14.39	3.0±0.2	6.09	18.11	7.36
[204]					4.73	21.28	15.83
[422]	23.07	35.63	48.38	35.1±0.45	58.12	82.84	67.93
[224]					56.85	79.86	59.99
[333]	16.56	24.27	34.35		39.14	57.07	44.56
[511]	16.58	24.25	34.34		39.75	58.05	47.73
[115]					37.93	55.14	39.78
[440]	20.69	32.07	44.05	32.2±0.4	52.59	75.97	63.99
[404]					51.09	72.41	54.43

[a]Reference 110.

HgTe),[107] and their direct observation in x-ray studies of charge densities (e.g., see Figs. 2 and 3 in Ref. 109).

F. X-ray scattering factors

The first four columns of Table IX show the calculated x-ray scattering factors $\rho(h,k,l)$ for ZnS, ZnSe, and ZnTe at the Miller indices h, k, and l allowed by the zinc-blende lattice (i.e., all even or all odd). The fifth column gives the observed[110] results for ZnSe (taking into account the Debye-Waller correction). The agreement with our calculation is very good. We are unaware of similar experimental results for ZnS and ZnTe and hence offer our calculated data (Table IX) as predictions.

G. Hydrostatic deformation potentials

Using our calculated band structure at different lattice parameters, we compute the deformation potentials

$$\gamma^{(i)}=\frac{dE^{(i)}}{d\ln\Omega}\ . \tag{30}$$

Table X depicts the calculated deformation potentials for a few interband transitions i, where comparison with experiment[111–113] is also given. These are used below to calculate the volume deformation contribution [b_{VD} of Eq. (19b)] to the optical bowing.

V. ELECTRONIC STRUCTURE OF Zn_2SSe, Zn_2SeTe, AND Zn_2STe IN THE CuAu I STRUCTURE

A. Band structures

Figure 10 depicts the band structures of the three equimolar ordered alloys Zn_2SSe, Zn_2SeTe, and Zn_2STe in the CuAu I–like structure, using the structural parameters of Table III. Table XI gives the band energies at high-symmetry points. At the limit $A=B$, $u=\frac{1}{4}$, and $c/a=1$, the CuAu I unit cell corresponds exactly to a doubling of the zinc-blende unit cell along the c axis. As such, the states of the CuAu I structure can be traced to those of the ZB structure by folding of the Brillouin zones [Eq. (28)]. The splitting of such states in the actual ABC_2 band structure represents the electronic disparity between A and B. Figure 10 shows a few such instances.

TABLE X. Calculated and observed hydrostatic deformation potentials [Eq. (30)] for ZnS, ZnSe, and ZnTe.

System	$\Gamma_{15v}\rightarrow\Gamma_{1c}$ Expt. (eV)	$\Gamma_{15v}\rightarrow\Gamma_{1c}$ Calc. (eV)	$\Gamma_{15v}\rightarrow X_{1c}$ Expt. (eV)	$\Gamma_{15v}\rightarrow X_{1c}$ Calc. (eV)	$\Gamma_{15v}\rightarrow\Gamma_{15c}$ Calc. (eV)
ZnS	4.0[a]	4.0	−1.4[c]	−1.8	+0.2
ZnSe	5.4[a]	4.2		−2.0	0.0
ZnTe	5.8[b]	5.8		−2.5	−1.0

[a]Reference 111.
[b]Reference 112.
[c]Reference 113.

(i) The bottom Γ_{1v} of the valence band of ABC_2 at $\bar{\Gamma}$ shows two distinct bands, corresponding roughly to the A and B anion s bands. The corresponding charge densities are shown for $SSeZn_2$ in Fig. 4(b) (the $\bar{\Gamma}_{1v}$ state derived from the ZB Γ_{1v} state) and Fig. 4(e) (the $\bar{\Gamma}_{1v}$ state derived from the ZB X_{1v} state). Clearly the lowest band has more amplitude on the S site. This asymmetry becomes very pronounced in $SeTeZn_2$ [see Fig. 6(b) for $\bar{\Gamma}_{1v}(\Gamma_{1v})$ and Fig. 6(e) for $\bar{\Gamma}_{1v}(X_{1v})$] and for $STeZn_2$ [see Fig. 8(b) for $\Gamma_{1v}(\Gamma_{1v})$ and Fig. 8(e) for $\bar{\Gamma}_{1v}(X_{1v})$]. In contrast, a VCA description results in a single anion s band at Γ, representing approximately the *average* of Γ_{1v} of the two constituents. While a VCA description does produce a splitting between Γ_{1v} and X_{1v}, this splitting does not reflect the disparity between the two anions. Instead, it reflects the fact that whereas Γ_{1v} is a pure (average) anion state, X_{1v} can mix in some *cation p* character. We find that the Γ_{1v}-X_{1v} splitting for ZnS, ZnSe, and ZnTe is 1.1±0.1 eV (Table VII), and that b_S and b_{CE} (both due to non-VCA effects) are the largest contributions to the relative b_I for these states, particularly in $SeTeZn_2$ and $STeZn_2$ (Table XII). Hence VCA for the alloys is expected to produce a similar ($\sim$1.1 eV) splitting. When the average VCA alloy is ordered, the Γ_{1v} and X_{1v} VCA states map into the two $\bar{\Gamma}_1$ states of CuAu I (lowest two bands in Fig. 10). The *excess* splitting of these two states (beyond the VCA Γ_{1v}-X_{1v} splitting) now reflects the potential difference between the anions. We find this $\bar{\Gamma}_{1v}(\Gamma_{1v})$-to-$\bar{\Gamma}_{1v}(X_{1v})$ splitting to be (Table XI) 1.2, 2.4, and 2.6 eV for Zn_2SSe, Zn_2SeTe, and Zn_2STe, respectively, i.e., considerably larger than the expected VCA value (1.1 eV) for the last two systems. There can be no doubt that the VCA description of such states as having equal amplitudes on both anion sites is invalid. Such large additional splitting could be observable in photoemission experiments (none are available for these systems, to our knowledge).

(ii) At the bottom of the VB at $\bar{M}$, two equivalent zinc-blende X_{1v} states fold in (and split) to form the nondegenerate $\bar{M}_1$ and $\bar{M}_2$ states. The splitting is found to be 0.4, 2.4, and 2.7 eV in Zn_2SSe, Zn_2SeTe, and Zn_2STe, respectively. (Note, however, that the doubly degenerate $\bar{M}$ state just above the Zn 3d band, arising from the folding of the zinc-blende X_3 states, does not split either in

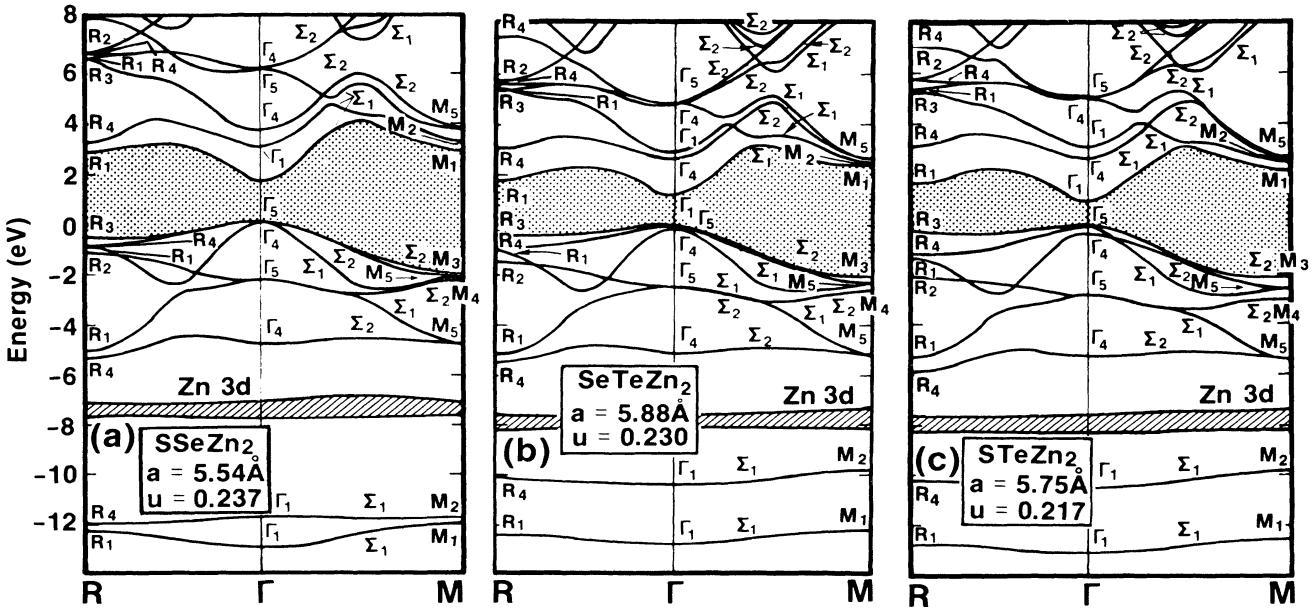

FIG. 10. Calculated nonrelativistic self-consistent band structures for (a) $SSeZn_2$, (b) $SeTeZn_2$, and (c) $STeZn_2$ in the CuAu I–like structure (Fig. 1), using the Ceperley-Alder exchange correlation. Origin of the coordinate system is S [part (a)], Se [part (b)], and S [part (c)]. Shaded areas denote the band-gap region. The symmetry labels are defined in Tables IV–VI and Ref. 88(b).

TABLE XI. Calculated band eigenvalues at the $\bar{\Gamma}$ point in the CuAu I Brillouin zone (in eV), relative to the valence-band maximum. The zinc-blende labels of the various levels are used to illustrate how the $\Gamma+X$ levels of ZB map into the $\bar{\Gamma}$ point of CuAu-I. Degeneracies are indicated in parentheses. Values of u_{eq} are from Table III. The Zn 3s and Zn 3p energies are -121.02 and -78.79 in ZnS, -121.29 and -79.04 in ZnSe, and -121.86 and -79.60 in ZnTe.

Level (ZB labels)	Zn_2SSe $u=\frac{1}{4}$	Zn_2SSe u_{eq}	Zn_2SeTe $u=\frac{1}{4}$	Zn_2SeTe u_{eq}	Zn_2STe $u=\frac{1}{4}$	Zn_2STe u_{eq}
Core levels						
Zn 3s(2)	−121.12	−121.17	−121.63	−121.71	−121.58	−121.76
Zn 3p(6)	−78.87	−78.92	−79.38	−79.44	−79.33	−79.52
s bands						
$\Gamma_{1v}(1)$	−12.96	−13.01	−12.34	−12.77	−12.31	−13.12
$X_{1v}(1)$	−11.79	−11.85	−10.59	−10.36	−10.77	−10.49
Zn d bands						
Γ_{15v} $\bar{\Gamma}_{4v}(1)$	−7.74	−7.78	−8.11	−8.18	−8.17	−8.34
Γ_{15v} $\bar{\Gamma}_{5v}(2)$	−7.73	−7.78	−8.08	−8.16	−8.15	−8.30
$X_{3v}(1)$	−7.60	−7.65	−8.03	−8.12	−7.98	−8.19
$X_{5v}(2)$	−7.49	−7.53	−7.87	−7.96	−7.91	−8.07
Γ_{12v} $\bar{\Gamma}_{1v}(1)$	−7.35	−7.40	−7.94	−8.03	−7.82	−8.04
Γ_{12v} $\bar{\Gamma}_{3v}(1)$	−7.35	−7.40	−7.93	−7.98	−7.80	−8.02
$X_{4v}(1)$	−7.29	−7.33	−7.86	−7.91	−7.77	−7.98
$X_{1v}(1)$	−7.08	−7.12	−7.45	−7.49	−7.45	−7.61
Upper VB						
$X_{3v}(1)$	−4.79	−4.84	−5.01	−5.10	−5.01	−5.23
$X_{5v}(2)$	−2.23	−2.33	−2.24	−2.46	−2.28	−2.81
Γ_{15v} $\bar{\Gamma}_{4v}(1)$	+0.01	−0.06	−0.05	−0.14	−0.11	−0.37
Γ_{15v} $\bar{\Gamma}_{5v}(2)$	0.00	0.00	0.00	0.00	0.00	0.00
Conduction						
$\Gamma_{1c}(1)$	1.72	1.61	1.51	1.18	1.64	0.97
$X_{1c}(1)$	3.06	3.06	2.76	2.86	3.04	3.13
$X_{3c}(1)$	3.77	3.70	2.71	2.62	2.94	2.67
Γ_{15c} $\bar{\Gamma}_{4c}(1)$	6.11	6.08	4.97	4.85	5.28	5.02
Γ_{15c} $\bar{\Gamma}_{5c}(2)$	6.11	6.07	4.92	4.87	5.20	5.04

VCA or in the ordered compound considered here.)

(iii) The lowest conduction bands at the $\bar{R}$ point (derived from the ZB L point) show a large $\bar{R}_1$-$\bar{R}_4$ splitting of 0.37 eV in $SSeZn_2$, 1.19 eV in $SeTeZn_2$, and 1.59 eV in $STeZn_2$.

The splittings noted in (ii) and (iii) would vanish in the VCA. Their experimental observation could therefore serve as an indication of ordering.

(iv) The valence-band maximum at $\bar{\Gamma}$ consists in ABC_2 of the crystal-field split $\bar{\Gamma}_{5v}$ (doubly degenerate) and $\bar{\Gamma}_{4v}$ (singly degenerate), both arising from the zinc-blende Γ_{15v} state (triply degenerate). Since the $\bar{\Gamma}_{5v}$-$\bar{\Gamma}_{4v}$ splitting is rather small (≤ 0.004 eV, see Table XI), its resolution may be obscured both by spin-orbit and alloy broadening effects.

B. Charge distribution

Figure 11 depicts the total electronic charge density of $SSeZn_2$, $SeTeZn_2$ and $STeZn_2$ in the (110) plane. They appear similar to a superposition of the valence charges of the constituent binary semiconductors displayed in Fig. 3. The picture changes qualitatively when one considers the charge densities of individual bands (Figs. 4–9). We see strong localization effects on individual anion sublattices, which breaks the tetrahedral site symmetry assumed in VCA models. In particular, the CBM at $\bar{\Gamma}_{1c}$ acquires in addition to its s character (characteristic of the ZB constituents) also some anion p character (through mixing with the unperturbed Γ_{15v} state of the ZB partners) and the $\bar{\Gamma}_{1c}(X_{1c})$ and $\bar{\Gamma}_{4c}(X_{3c})$ states show strong cross-hybridization of s and p character. Indeed the $\bar{\Gamma}_{1c}(X_{1c})$ and $\bar{\Gamma}_{4c}(X_{3c})$ states have almost lost in the ternary system all resemblance to their parent states in the ZB constituents.

C. X-ray scattering factors

Using the atomic positions in the CuAu I structure given in Eq. (25) and the reciprocal lattice vectors corresponding to Eq. (24), the x-ray structure factor for this ABC_2 unit cell is given as

$$S_{\mathrm{CuAu}}(\mathbf{G})=\tfrac{1}{2}[f_A+f_B e^{-i\pi(h+\eta l)} + f_C e^{-i(\pi/2)(h+k+4u\eta l)}(1+e^{-i\pi(h-4u\eta l)})] \times(1+e^{-i\pi(h+k)}) . \quad (31)$$

Here, h, k, and l are indices along Cartesian axes such that h, k, and ηl are integers, $\eta = c/a$, and the cation displacement parameter u is given by Eq. (27). In the "ideal" CuAu I structure, $\eta = 1$ and $u = \frac{1}{4}$. This structure becomes the (double) zinc-blende lattice for $A = B$ (where also $\eta = 1$ and $u = \frac{1}{4}$). f_A, f_B, and f_C are atomic structure factors. Nonzero reflections are seen to occur only if h and k are both odd or both even. In the zinc-blende (as well as the VCA) limit where $\langle AB \rangle$ replaces A and B, Eq. (31) becomes

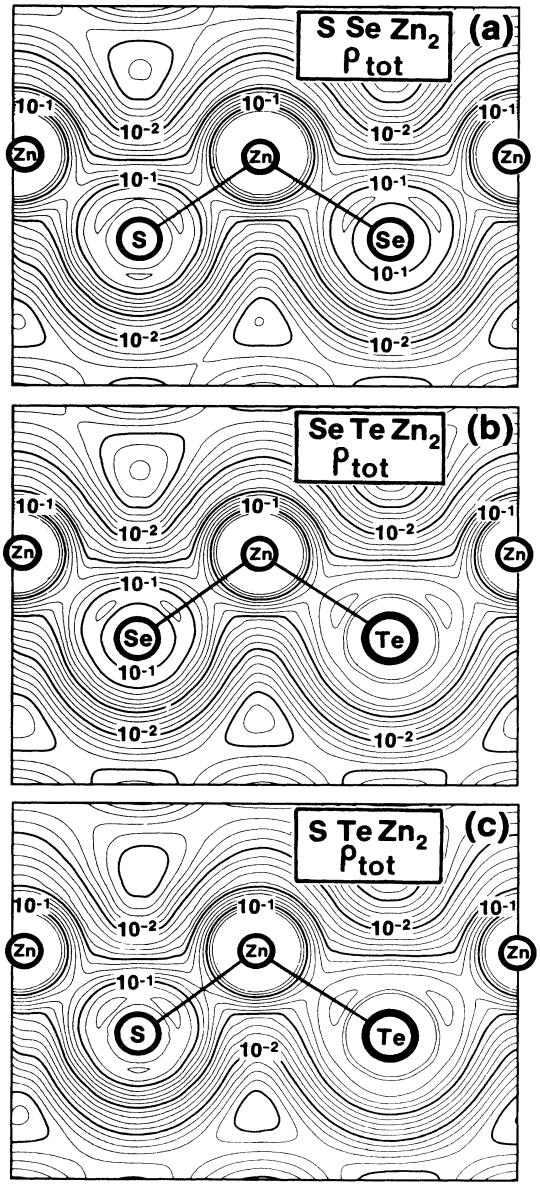

FIG. 11. Total valence-band charge density in relaxed (a) $SSeZn_2$, (b) $SeTeZn_2$, and (c) $STeZn_2$. The contours are displayed in the (110) plane, are logarithmically spaced, and are given in units of e/a.u.[3]

$$S_{\mathrm{ZB}}(\mathbf{G}) = \tfrac{1}{4}(f_{\langle AB \rangle} + f_C e^{-i(\pi/2)(h+k+l)}) \times (1 + e^{-i\pi(h+k)} + e^{-i\pi(h+l)} + e^{-i\pi(k+l)}) \quad (32)$$

The factor to the right vanishes unless h, k, and l are all odd or all even. We refer to this set of reflections as "group (i)," or "zinc-blende allowed," and give their calculated values for ZnS, ZnSe, and ZnTe, as well as for their 50%-50% binary alloys in Table VI. Note also that for zinc-blende materials there is a degeneracy $S_{\mathrm{ZB}}(h,k,l) = S_{\mathrm{ZB}}(k,l,h) = S_{\mathrm{ZB}}(h,l,k)$, whereas for group (i) reflections in the CuAu I structure [i.e., u, η general, $A \neq B$, but $(h,k,\eta l)$ are all odd or all even] we have

$$S^{(\mathrm{i})}_{\mathrm{CuAu}}(\mathbf{G}) = f_A + \tfrac{1}{2} f_C e^{-i(\pi/2)(h+k+4u\eta l)} \times (1 + e^{-i\pi(h-4u\eta l)}) + f_B + \tfrac{1}{2} f_C e^{-i(\pi/2)(h+k+4u\eta l)} \times (1 + e^{-i\pi(h-4u\eta l)}) , \quad (33)$$

hence this degeneracy is lifted (see Table IX). For $u = \frac{1}{4}$ and $\eta = 1$, this reduces to the scattering factors of the zinc-blende components AC and BC. For $u = \frac{1}{4}$, all group-(i) reflections with the same $h+k+l$ have the same scattering factor. All reflections of the CuAu I structure that are not part of group (i) are referred to as "group (ii)," or "zinc-blende forbidden." They include the (even,even,odd) and (odd,odd,even) cases, and are given in Table XIII for both $u = \frac{1}{4}$ and for the equilibrium value u_{eq} (Table III). The general expression for group-(ii) reflections is

$$S^{(\mathrm{ii})}_{\mathrm{CuAu}}(\mathbf{G}) = f_A - f_B + f_C e^{-i(\pi/2)(h+k+4u\eta l)} \times (1 + e^{-i\pi(h-4u\eta l)}) . \quad (34)$$

For $u = \frac{1}{4}$ and $\eta = 1$, group-(ii) reflections reduce to

$$S^{(\mathrm{ii})}_{\mathrm{CuAu}}(\mathbf{G}) = f_A - f_B ; \quad u = \tfrac{1}{4}, \ \eta = 1 , \quad (35)$$

and hence provide a direct measure of the chemical disparity of the alloyed elments. Note also that the phase of $S(\mathbf{G})$ is unimportant although the relative phases of the component terms may substantially affect the magnitude of $S(\mathbf{G})$. An interesting consequence occurs, for example, for group-(i) reflections when $u = \frac{1}{4}$ and $\eta = 1$ in the CuAu I structure. According to Eq. (33), for this case

$$S^{(\mathrm{i})}(\mathbf{G}) = (f_A + f_C e^{-i(\pi/2)(h+k+l)}) + (f_B + f_C e^{-i(\pi/2)(h+k+l)}) . \quad (36)$$

The phase factor is -1 when $h+k+l = 2(2j+1)$, where j is an integer. In this case the magnitude of $S(\mathbf{G})$ is

$$S(\mathbf{G}) = | f_A + f_B - 2f_C | , \quad (37)$$

which is equal to the magnitude of the difference of the magnitudes of $S_{\mathrm{ZB}}(\mathbf{G})$ for AC and BC if either $f_A - f_C$ or $f_B - f_C$ is negative.

TABLE XII. Calculated bowing parameters, showing the volume deformation [VD, Eq. (19b)], chemical electronegativity [CE, Eq. (20b)], and structural [S, Eq. (21b)] components and the total bowing b_I of the ordered structure [Eq. (23)]. Bowing is given relative to the $\bar{\Gamma}_5$ top of the valence band.

Level (ZB label)	ZnS_xSe_{1-x}				$ZnSe_xTe_{1-x}$				ZnS_xTe_{1-x}			
	b_{VD}	b_{CE}	b_S	b_I	b_{VD}	b_{CE}	b_S	b_I	b_{VD}	b_{CE}	b_S	b_I
Core levels												
Zn 3*s*(2)	0.03	−0.17	0.19	0.05	0.35	−0.10	0.29	0.54	0.64	−0.09	0.74	1.29
Zn 3*p*(6)	0.00	−0.16	0.18	0.03	0.33	−0.09	0.29	0.53	0.64	−0.09	0.74	1.29
s bands												
$\Gamma_{1v}(1)$	−0.03	0.04	0.20	0.21	0.24	1.07	1.74	3.05	0.35	0.46	3.23	4.04
$X_{1v}(1)$	−0.06	−0.11	0.22	0.06	0.11	−1.26	−0.94	−2.10	0.25	−0.85	−1.16	−1.76
Zn *d* bands												
Γ_{15v} $\bar{\Gamma}_{4v}(1)$	−0.02	−0.05	0.18	0.11	0.10	0.08	0.27	0.45	0.74	0.10	0.70	1.54
Γ_{15v} $\bar{\Gamma}_{5v}(2)$	−0.02	−0.06	0.20	0.11	0.10	−0.03	0.31	0.39	0.74	0.02	0.59	1.36
$\Gamma_{12v}(2)$	−0.05	−0.09	0.20	0.06	0.54	−0.04	0.28	0.77	0.47	−0.03	0.87	1.31
$X_{5v}(2)$	0.01	−0.09	0.17	0.09	0.07	−0.06	0.38	0.39	0.67	−0.07	0.64	1.24
Upper VB												
$X_{3v}(1)$	−0.02	−0.04	0.19	0.12	0.14	−0.03	0.35	0.46	0.28	−0.12	0.89	1.05
$X_{5v}(2)$	−0.02	−0.05	0.40	0.33	0.10	−0.05	0.85	0.90	0.16	−0.15	2.12	2.13
Γ_{15v} $\bar{\Gamma}_{4v}(1)$	0.0	−0.03	0.28	0.25	0.00	0.18	0.39	0.57	0.00	0.43	1.07	1.50
Γ_{15v} $\bar{\Gamma}_{5v}(2)$	0.0	0.0	0.0	0.0	0.0	0.0	0.0	0.0	0.0	0.0	0.0	0.0
Conduction												
$\Gamma_{1c}(1)$	−0.10	0.03	0.45	0.39	−0.36	1.00	1.32	1.96	−0.54	1.68	2.68	3.83
$X_{1c}(1)$	−0.02	−0.08	−0.01	−0.11	0.09	−0.93	−0.39	−1.22	0.20	−1.54	−0.37	−1.71
$X_{3c}(1)$	0.07	−0.08	0.29	0.28	0.34	0.00	0.35	0.69	0.81	−0.19	1.08	1.70
Γ_{15c} $\bar{\Gamma}_{4c}(1)$	0.03	−0.03	0.13	0.12	0.19	−0.11	0.50	0.57	0.43	−0.23	1.03	1.24
Γ_{15c} $\bar{\Gamma}_{5c}(2)$	0.03	−0.03	0.17	0.17	0.19	0.08	0.23	0.49	0.43	0.08	0.63	1.14

TABLE XIII. Calculated electronic x-ray structure factors (in e/mol) for group-(ii) reflections [Eq. (34)], i.e., the superstructure reflections which vanish in the zinc-blende limit. Origin at the X anion in the Zn_2XY ternary.

	Zn_2Se		Zn_2SeTe		Zn_2STe	
Beam	u_{eq}	$u=\frac{1}{4}$	u_{eq}	$u=\frac{1}{4}$	u_{eq}	$u=\frac{1}{4}$
[001]	12.81	17.37	10.04	16.95	22.75	34.32
[110]	16.87	16.87	16.20	16.19	33.07	33.07
[201]	19.67	15.76	20.71	14.70	40.49	30.48
[112]	17.20	15.47	18.41	14.38	35.34	29.88
[003]	25.09	14.65	29.43	13.48	53.71	28.19
[221]	11.15	14.67	8.11	13.55	19.25	28.27
[310]	14.41	14.42	13.25	13.26	27.74	27.73
[203]	4.19	13.73	2.03	12.63	3.05	26.44
[312]	14.89	13.50	15.79	12.43	30.50	26.03
[401]	9.92	12.88	7.24	11.86	17.21	24.86
[223]	21.70	12.89	25.50	11.88	46.57	24.89
[330]	12.68	12.66	11.73	11.70	24.52	24.51
[114]	17.07	12.69	21.06	11.69	36.41	24.51
[332]	13.12	11.97	13.94	11.10	26.98	23.20
[421]	14.88	12.12	15.56	11.24	30.64	23.50
[403]	19.10	11.45	22.65	10.71	41.27	22.32
[005]	1.08	11.43	8.39	10.68	5.66	22.29
[314]	15.07	11.29	18.71	10.58	32.34	22.04
[510]	11.27	11.26	10.59	10.58	22.03	22.02
[423]	3.62	10.82	1.02	10.25	3.40	21.26
[205]	22.61	10.83	28.28	10.26	47.65	21.27
[512]	11.69	10.68	12.62	10.16	24.30	21.03

Observation of group (ii) reflections in pseudobinary alloys of zinc-blende components can serve as an indication of ordering. Such reflections were recently observed for GaAs-AlAs alloys.[77]

VI. OPTICAL BOWING

A. The single-cluster ABC_2 model

Table XII depicts our calculated bowing coefficients for ZnS_xSe_{1-x}, $ZnSe_xTe_{1-x}$, and ZnS_xTe_{1-x} using the ordered ABC_2 structure as a model for the 50%-50% alloy. We also give the breakdown of the total bowing b into its volume deformation [Eq. (19b)], chemical electronegativity [Eq. (20b)], and structural [Eq. (21b)] components.

A few conclusions are apparent.

(i) Relaxing the cell-internal degrees of freedom (u) increases the bowing b: The structural contribution b_S is generally positive, and overwhelms the other two contributions.[114] It correlates with the atomic size mismatch of the alloyed atoms, i.e., using Pauling's tetrahedral radii of 1.04, 1.14, and 1.32 Å for S, Se, and Te, respectively, the S-Se and Se-Te and S-Te size mismatches are 0.10, 0.18, and 0.28 Å, respectively, hence b_S(S-Se) $< b_S$(Se-Te) $< b_S$(S-Te).

(ii) The chemical electronegativity contribution b_{CE} is generally (but not always) negative and scales with the electronegativity mismatch of the alloyed atoms. Using Pauling's electronegativities of 2.5, 2.4, and 2.1 for S, Se, and Te, respectively, we have an electronegativity mismatch of 0.1, 0.3, and 0.4 for S-Se, Se-Te, and S-Te, respectively, hence $|b_{CE}(\text{S-Te})| > |b_{CE}(\text{S-Se})|$.

(iii) The volume deformation contribution b_{VD} is positive for the S-Te system, having the largest lattice constant mismatch, and is far smaller for the S-Se system with the smallest lattice constant mismatch in this series. These findings suggest that the order contribution $b_I = b_{VD} + b_{CE} + b_S$ to the total bowing scales both with the electronegativity difference $\Delta\chi_{AB}$ and with the atomic size difference ΔR_{AB}. In fact, a plot of b versus $\Delta\chi_{AB}\Delta R_{AB}$ for II-VI and III-V alloys is nearly linear, with an intercept at zero. This suggests that previous claims[40] that the scaling of b with $\Delta\chi$ are indicative of disorder effects (as suggested by Van Vechten and Berstresser[38]) are not well founded.

(iv) The bowing parameters $b_{n\mathbf{k}}$ of Table X were given relative to the top of the valence band (the $\bar{\Gamma}_{5v}$ state). These $b_{n\mathbf{k}}$(VBM) values could easily be converted to bowing parameters $\tilde{b}_{n\mathbf{k}}$(core) relative to deep core states (e.g., the Zn $3s$ or Zn $3p$) simply by noting that

$$\tilde{b}_{n\mathbf{k}}(\text{core}) = b_{n\mathbf{k}}(\text{VBM}) - b_{\text{core}}(\text{VBM}) \ . \tag{38}$$

For example, using for $n\mathbf{k}$ the X_{5v} state and the Zn $3s$ core, we have $\tilde{b}$ values from Table X of $0.33-0.05=0.28$ eV, $0.90-0.54=0.36$ eV, and $2.13-1.29=0.84$ eV for ZnS_xSe_{1-x}, $ZnSe_xTe_{1-x}$, and ZnS_xTe_{1-x}, respectively. In the particular case where $n\mathbf{k}$ is the $\bar{\Gamma}_{5v}$ state we see that the bowing of the VBM relative to the deep core states is simply $-b_{\text{core}}(\text{VBM})$. Hence *we predict a negative bowing of the VBM* of -0.05, -0.29, and -1.29 eV for ZnS_xSe_{1-x}, $ZnSe_xTe_{1-x}$, and ZnS_xTe_{1-x}, respectively. In contrast, Table X shows that for all valence states $n\mathbf{k}$ (except X_{3v} for ZnS_xTe_{1-x}) one has $b_{n\mathbf{k}}(\text{VBM}) > b_{\text{core}}(\text{VBM})$, hence we predict *positive* bowing of valence-band states with respect to core states. This prediction awaits testing by core photoemission experiments.

It is interesting to observe that the bowing parameters of the deep core states of the different common cation states (e.g., Zn $3s$, Zn $3p$) are nearly equal in each alloy. Furthermore, we find from Table XI that the difference between the Zn $3s$ and Zn $3p$ band energies is nearly the same in all materials, e.g., 42.23 eV in ZnS, 42.25 eV in ZnSe, 42.26 eV in ZnTe, 42.25 eV in $SSeZn_2$, 42.23 eV in $SeTeZn_2$, and 42.23 eV in $STeZn_2$. This suggests the possibility that these core states are placed at the same energy separation from the intrinsic vacuum level in all of these materials (note that this is simply a particular example of the "vacuum pinning rule" for impurities suggested by Caldas *et al.*[115,116]). Hence, differences in core binding energies (relative to their VBM) of two materials can be used to approximate the intrinsic valence-band offsets.

It is interesting to note how the different contributions to the bowing affect the various band states. Figures 12–14 depict the variation of various high-symmetry band energies with volume deformation and structural relaxation. Considering the ZnS-ZnTe example of Fig. 14, we see that dilating ZnS from its equilibrium lattice parameter to that pertaining to $STeZn_2$ causes an upward shift of its bonding valence-band states (relative to the VBM) and a downward shift in the antibonding conduction bands (except X_{1c} which has an inverted deformation potential; see Table X). The band energies of ZnTe respond to *compression* of the lattice parameter in just the opposite way: The valence-band energies shift downwards and the Γ_{1c} conduction band shifts upwards. Note that ZnTe becomes an indirect-gap semiconductor under such a compression (Figs. 13 and 14). The *relative* hydrostatic deformation potentials [Eq. (19c)] then determine whether b_{VD} is positive (most states in ZnSe-ZnTe and ZnS-ZnTe, see Table X), or negative (most states in ZnS-ZnSe). Having prepared ZnS and ZnTe in their final equilibrium volume, we now bring the two constituents together to form the relaxed alloy. Figures 12–14 (center panel) then show how the prepared states interact: The Γ_{1c} state of compressed ZnTe is lowered substantially by interacting with the Γ_{1c} state of dilated ZnS which is nearly unshifted. This asymmetry contributes largely to the optical bowing of Zn_2STe. Note that the interaction of the compressed and dilated ZB bands almost always repels them in *opposite* directions, resulting in a *positive* contribution to the bowing. In contrast, the prepared X_{1v} states in ZnS-ZnTe and ZnSe-ZnTe are pushed in the same (upward) direction, resulting in a *negative* bowing.

To summarize our predicted bowing parameters, we show in Fig. 15 the variation of the lowest $\Gamma_{15v} \rightarrow \bar{\Gamma}_{1c}(\Gamma_{1c})$, $\Gamma_{15v} \rightarrow \bar{\Gamma}_{1c}(X_{1c})$, $\Gamma_{15v} \rightarrow \bar{\Gamma}_{4c}(X_{3c})$, and $\Gamma_{15v} \rightarrow \bar{\Gamma}_{5c}(\Gamma_{15c})$ band gaps in alloys of ZnS-ZnSe-ZnTe using for the end-point materials the best-known values (rather than those obtained by the density-functional calculation).

We will now consider in greater detail the individual contributions b_{S} and b_{VD} to b_{I}. The structural-relaxation contribution can be expanded in a power series:

$$b_{\text{S}} = \alpha_{A,B,C}(u-\tfrac{1}{4}) + \beta_{A,B,C}(u-\tfrac{1}{4})^2 + \cdots . \tag{39}$$

If A and B are interchanged, and $(u-\frac{1}{4})$ is replaced by $(\frac{1}{4}-u)$, the energy levels (and b_{S}) of ABC_2 must remain unchanged. Thus, α is antisymmetric and β is symmetric under this operation. In the simple limit of a zinc-blende compound where $A=B$, this result can hold only if α vanishes. Hence α must depend on the *difference* between A and B, so that Eq. (39) can be written as

$$b_{\text{S}} = \alpha_{A-B}(u-\tfrac{1}{4}) + \beta_{A+B}(u-\tfrac{1}{4})^2 + \cdots , \tag{40}$$

where we indicate the symmetric nature of β by the sum

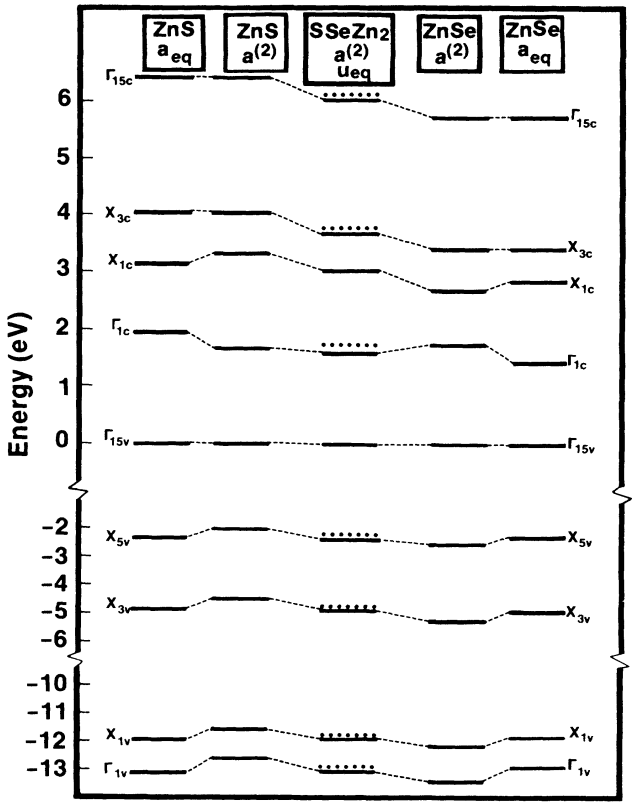

FIG. 12. Variation of band energies of ZnS and ZnSe at high-symmetry points showing the stepwise formation of the states of the ordered alloy.

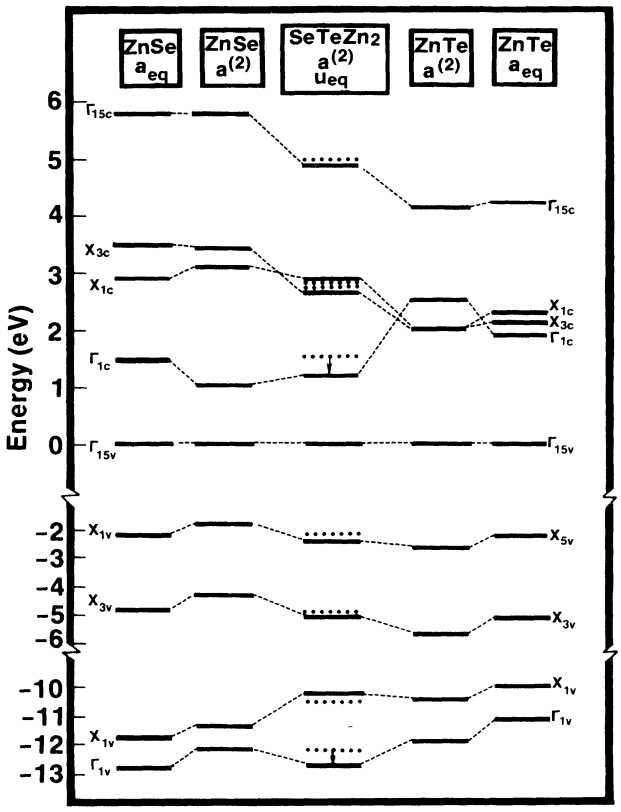

FIG. 13. The same as Fig. 12, for ZnSe and ZnTe.

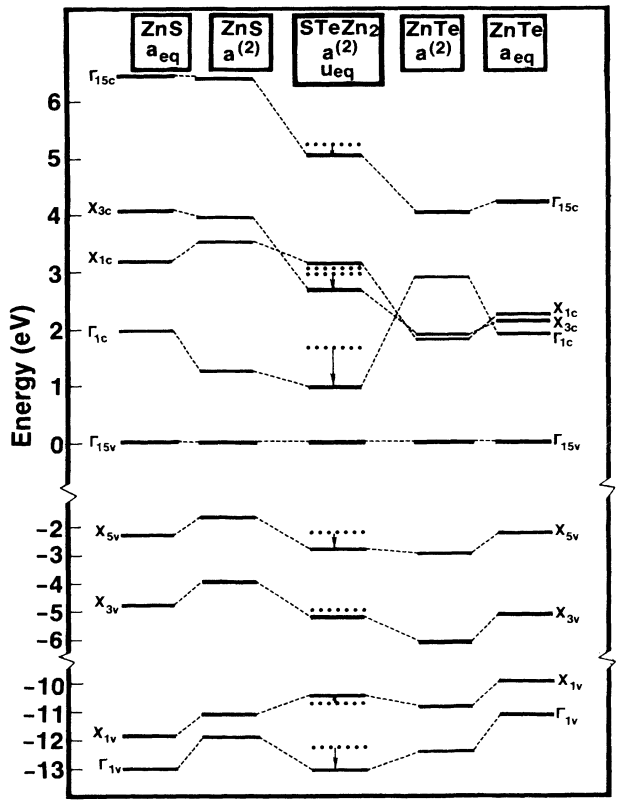

FIG. 14. The same as Fig. 12, for ZnS and ZnTe.

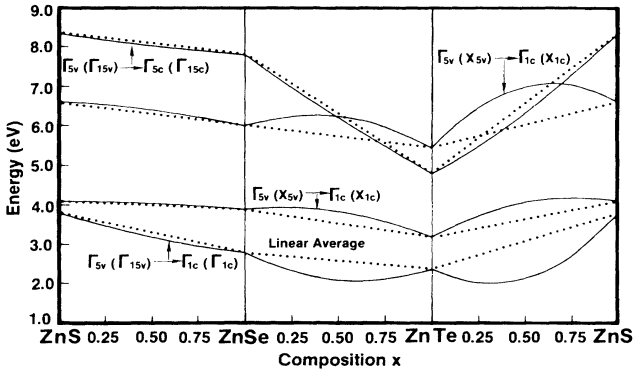

FIG. 15. Predicted variation of the few lowest interband transition energies in ZnS-ZnSe-ZnTe alloys, using our calculated bowing parameters (Table XII) and the experimental band gaps of the end-point materials.

$A+B$ in the subscript.

It is also worth noting that for $u=u_{\rm eq}^{(2)}$, $c/a=1$, and R_{AC} and R_{BC} near their ideal (zinc-blende) values we have

$$u-\tfrac{1}{4}\sim\sqrt{3}(R_{AC}-R_{BC})/2a\ . \tag{41}$$

Hence Eqs. (39) and (40) are equivalent to an expansion in powers of the lattice mismatch, $\Delta R/a$.

It is interesting that in nearly all cases b_S is positive (Table XII), the exceptions being the $\overline{\Gamma}_{1v}(X_{1v})$ and $\overline{\Gamma}_{1c}(X_{1c})$ states in Zn_2SeTe and Zn_2STe, and the $\overline{\Gamma}_{1c}(X_{1c})$ state in Zn_2SSe. An examination of the band-by-band charge-density plots (Figs. 8 and 9) suggests the reasons for this. For purposes of discussion, we will consider the case of Zn_2STe, Figs. 8(b), 8(e), 9(b), and 9(e). In the $\overline{\Gamma}_{1v}(\Gamma_{1v})$ state the majority of the charge resides in the ZnS bond, and very little charge resides in the ZnTe bond. This asymmetry is the major contributor to b_S for this state. We should point out the reduction of the u parameter from $\frac{1}{4}$ to $u_{\rm eq}$ of the CuAu I structure results in bringing the center and leftmost Zn atoms in the charge-density plots closer together, while the center and rightmost Zn atoms move farther apart. In a zinc-blende compound (AAC_2), which has a *symmetric* charge distribution (since $u_{\rm eq}=\frac{1}{4}$), reduction of u would raise the energy of the rightmost AC bond and lower that of the leftmost AC bond by an approximately compensating amount, resulting in relatively little change in the band energy of the $\overline{\Gamma}_{1v}$ state relative to that of the top of the valence band (which also has symmetric charge density). Thus one would expect $\alpha_{A-B}=0$ and $\beta_{A+B}\ll 1$; hence $b_S\cong 0$ in that case. In contrast in Zn_2STe, the large asymmetry between the Zn—S and Zn—Te bonds would cause the band energy of $\overline{\Gamma}_{1v}(\Gamma_{1v})$ to drop (relative to the more symmetric VB maximum) as u is reduced below $\frac{1}{4}$, since the energy in the Zn—S bond will drop by a much larger amount than the energy of the Zn—Te bond increases. Thus, the bowing should be large and positive. In contrast, the $\overline{\Gamma}_{1v}(X_{1v})$ state is complementary to $\overline{\Gamma}_{1v}(\Gamma_{1v})$ in that the

majority of the charge lies in the Zn—Te bond, with much less in the Zn—S bond. Hence, the bowing should be negative in this state.

In the conduction bands, a slightly different argument must be used since the states are antibonding between nearest-neighbor atoms. Here the large interstitial charge density provides an *attractive* force between pairs of Zn atoms. In the zinc-blende case, the symmetry results in compensating energy changes with changes in u, so that $b_S \approx 0$ as in the valence states. In Zn_2STe the large asymmetry in $\bar{\Gamma}_{1c}(\Gamma_{1c})$ causes the energy (relative to the VB maximum again) to drop with decreasing u, since the largest portion of the charge lies between the leftmost pair of Zn atoms. Thus, this state should exhibit positive b_S. The $\bar{\Gamma}_{1c}(X_{1c})$ state is complementary, having most of its charge between the rightmost pair of Zn atoms, so that its b_S is negative.

These arguments hold as well in Zn_2SeTe, but for the state $\bar{\Gamma}_{1v}(X_{1v})$ in Zn_2SSe other effects apparently dominate, since the states are much more nearly symmetric.

The volume-deformation contribution b_{VD} has been given in terms of deformation potentials previously [Eq. (19c)]. Values calculated from the deformation potentials shown in Table X typically agree with those calculated directly from Eq. (19b) to within 20% for Zn_2SSe, 10% for Zn_2SeTe, and 1% for Zn_2STe.

B. Corrections due to multiple clusters

So far we have modeled the properties of the 50%-50% alloy by those of the ordered ABC_2 structure. As discussed in Sec. II A, part of the disparity between the calculated ordered contribution b_I (Table XII) and the experimental bowing b_{expt} (Table II) would arise from disorder, e.g., the existence at the composition $x=0.5$ of "minority clusters" AC, BC, A_3BC_4, and AB_3C_4 with nonvanishing probabilities $P^{(n)}(x,T)$. One could model this disorder contribution to the bowing by considering the band-gap energies $\varepsilon_g^{(n)}(A_nB_{4-n}C_4, a(0.5))$ of these clusters, evaluated at the 50%-50% alloy lattice parameter $a(0.5)$. We have carried out this procedure for $ZnS_{0.5}Te_{0.5}$ by calculating the band structures of ZnS, ZnTe, Zn_2STe, Zn_4S_3Te, and Zn_4STe_3 at the lattice parameter $a(0.5)=5.749$ Å. As before, we optimize all cell internal degrees of freedom at this lattice parameter, finding $u^{(3)}(0.5)=0.2681$ for Zn_4S_3Te and $u^{(1)}(0.5)=0.2328$ for Zn_4STe_3. The average band gap at $a=a(0.5)$ arising from these clusters is then

$$\varepsilon(0.5)=\sum_n P^{(n)}(x=0.5) \times \varepsilon_g^{(n)}(A_nB_{4-n}C_4, a(0.5), u^{(n)}(0.5)) , \quad (42)$$

where $P^{(n)}(x)$ are the occurrence probabilities at $x=0.5$.

The total bowing is calculated from Eq. (4) for state i as

$$b_{tot}^{(i)}=4[\tfrac{1}{2}\varepsilon^{(i)}(AC, a_{AC})+\tfrac{1}{2}\varepsilon^{(i)}(BC, a_{BC})-\varepsilon^{(i)}(0.5)] , \quad (43)$$

whereas the contribution of the minority clusters is simply the amount by which $b_{tot}^{(i)}$ deviates from $b_I^{(i)}$ [Eq. (23) and Table XII] calculated from ABC_2 alone:

$$b_{II}^{(i)}=b_{tot}^{(i)}-b_I^{(i)} . \quad (44)$$

The central difficulty in this procedure is the estimation of the probabilities $P^{(n)}(x)$ of occurrence of $A_nB_{4-n}C_4$ at a given composition. First-principles calculations of the phase diagram of lattice-mismatched alloys[74] indicate that $P^{(n)}(x)$ deviate substantially from the *random* (R) probabilities

$$P_R^{(n)}(x)=\binom{4}{n}x^n(1-x)^{4-n} . \quad (45)$$

To estimate, however, an *upper bound* for disorder contributions to b, we have used these random probabilities $P_R^{(n)}(x)$ in Eq. (45). We find for $ZnS_{0.5}Te_{0.5}$ the following results for the three lowest conduction states (using the same zinc-blende notation as in Table XII):

$$b_{tot}(\Gamma_{1c})=2.94 \text{ eV}, \quad b_{II}(\Gamma_{1c})=-0.89 \text{ eV} ;$$

$$b_{tot}(X_{1c})=-1.45 \text{ eV}, \quad b_{II}(X_{1c})=0.26 \text{ eV} ;$$

$$b_{tot}(X_{3c})=1.31 \text{ eV}, \quad b_{II}(X_{3c})=-0.39 \text{ eV} .$$

Note that disorder effects tend to raise the band gap, hence reducing the magnitude of the bowing parameters relative to the prediction of the completely ordered model. These results are in better agreement with experiment: $b_{expt}(\Gamma_{1c})$ of Table II is 3.0 eV, closer to $b_{tot}(\Gamma_{1c})=2.94$ eV than to the ordered contribution $b_I(\Gamma_{1c})=3.83$ eV of Table X. This would suggest a *maximum* contribution of disorder, in the extreme case of ZnS-ZnTe [having an enormous lattice mismatch, hence the largest deviations of $P^{(n)}(x)$ from $P_R^{(n)}(x)$] of $b_{II}(\Gamma_{1c})/b_{tot}(\Gamma_{1c})$ of 30%. We expect in general the disorder contribution to be considerably smaller, as the cluster probabilities $P^{(n)}(0.5)$ are considerably *smaller*[74] than $P_R^{(n)}(0.5)$ for all $n \neq 2$. Note that the *increase* in the lowest band gap (decrease of its bowing parameter) upon disordering of an ordered structure, evident in our results ($b_{II}<0$), is also observed experimentally in superlattices:[117] disordering of (ordered) III-V superlattices (catalyzed by introduction of a fast-diffusing impurity such as Zn) is indeed observed[117] to increase the band gap.

VII. SUMMARY AND CONCLUSIONS

We have presented first-principles calculations of the electronic structure of ZnS, ZnSe, and ZnTe in the zinc-blende structure, and Zn_2SSe, Zn_2SeTe, and Zn_2STe in a CuAu I–derived structure. The optical bowing in zinc chalcogenide alloys is well represented by the use of the ABC_2 ordered structure, which has the same local atomic arrangement as the predominant one in the alloy at composition $x=0.5$. We conclude that the disorder contribution b_{II} to the bowing parameter is small, particularly in the case of alloys with a large size mismatch, for which the tendency to order is strong. This is consistent with the results of CPA calculations, which show small disorder contributions in other alloy systems, as well as with the large disorder contributions required to fit experiment in earlier VCA-based calculations.

The "intrinsic" bowing b_I for many transitions involv-

ing the top of the valence band has been decomposed into three components, b_{VD}, b_{CE}, and b_S, showing that bowing arises principally from the structural relaxation b_S possible in locally ordered structures, with decreasing contributions (in order) due to charge exchange in the unrelaxed structure, b_{CE}, and volume deformation of the end-point compounds, b_{VD}. The origin of the structural-relaxation contribution b_S apparently lies in the fact that the asymmetry in the charge density in most of the individual valence and conduction states is greater than that of the valence-band maximum so that band energies with respect to the VB maximum change significantly in response to the structural relaxation. The asymmetry responsible for this is a manifestly non-VCA effect and increases with increasing size and electronegativity mismatch between the anions.

The folding of the bands of the zinc-blende structure into the smaller Brillouin zone of the CuAu I structure has implications which should be manifest in photoelectron spectroscopy experiments. For example, the folding of one of the zinc-blende X points into the zone center results in a pair of distinct bands at the bottom of the valence band at $\bar{\Gamma}$ having an energy difference of 2.6 eV in Zn_2STe, which should readily be measurable. Other measurable effects result from the splitting of states which would otherwise be degenerate (due to folding) if the two anions were identical (e.g., in the VCA). As an example, we cite the two lowest bands at $\bar{M}$ (derived from two of the zinc-blende X points), which are split by 2.7 eV in Zn_2STe.

As a consequence of the success of the ordered-structure approach used here, the VCA violations apparent in the charge-density plots and the band structures, and the empirical nature of the previous VCA-based calculations, we conclude that the success of some of the VCA calculations in reproducing the experimental bowing parameters is artificial, and that other applications of the VCA to semiconductor alloys should be re-examined.

ACKNOWLEDGMENT

This work was supported by the Office of Energy Research, Materials Science Division, U.S. Department of Energy, under Grant No. DE-AC02-77-CH00178.

[1]J. C. Woolley, in *Compound Semiconductors,* edited by R. K. Willardson and H. L. Goering (Reinhold, New York, 1962), p. 3.

[2]N. K. Abrikosov, V. F. Bankina, L. V. Poretskaya, L. E. Shelimova, and E. V. Skudnova, *Semiconducting II-VI, IV-V, and V-VI Compounds* (Plenum, New York, 1969).

[3]N. A. Goryunova, *The Chemistry of Diamond-Like Semiconductors* (MIT, Cambridge, 1963).

[4]A. N. Pikhtin, Fiz. Tekh. Poluprovodn. **11**, 425 (1977) [Sov. Phys.—Semicond. **11**, 245 (1977)].

[5]There are a number of interesting alloy systems which show structural phase transitions at some value of x. These include $(CdS)_x(ZnSe)_{1-x}$ (wurtzite) for $x>0.7$ [A. G. Fischer and R. J. Paff, J. Phys. Chem. Solids **23**, 1479 (1967)], $(CdSe)_x(CdTe)_{1-x}$ showing a zinc-blende to wurtzite transition at $x<0.3$ [A. D. Stuckes and G. Farrel, J. Phys. Chem. Solids **25**, 477 (1964)], and $(MnTe)_x(ZnTe)_{1-x}$ where a NaCl phase appears for 8–75% InTe, whereas neither GeTe nor InTe have a NaCl structure at low temperatures [J. C. Woolley, J. Electrochem. Soc. **11**, 906 (1965)].

[6]L. Végard, Z. Phys. **5**, 17 (1921).

[7]C. Y. Fong, W. Weber, and J. C. Phillips, Phys. Rev. B **12**, 5387 (1976).

[8]S. S. Vishnubhatla, B. Eyglunent, and J. C. Woolley, Can. J. Phys. **47**, 1661 (1968).

[9]D. Long, in *Semiconductors and Semimetals,* edited by R. K. Willardson and A. C. Beer (Academic, New York, 1966), Vol. 1, p. 143.

[10]O. Madelung, *Physics of III-V Compounds* (Wiley, New York, 1964), p. 269.

[11]M. Jaros, Rep. Prog. Phys. **48**, 1091 (1985).

[12]W. Czaja, Festkörperprobleme **11**, 65 (1971).

[13]N. O. Gavaleshko, W. Dobrowolski, M. Baj., L. Dmowski, T. Dietl, and V. V. Khomyak, in *Physics of Narrow Gap Semiconductors,* edited by J. Rauluszkiewicz, M. Gorska, and E. Kaczmarek (Elsevier, Amsterdam, 1978), p. 331.

[14]A. Ebina, Y. Sato, and T. Takahashi, Phys. Rev. Lett. **32**, 1366 (1974).

[15]P. Parayanthal and F. H. Pollak, Phys. Rev. **28**, 3632 (1983).

[16]J. A. Van Vechten, O. Berolo, and J. C. Woolley, Phys. Rev. Lett. **29**, 1400 (1972).

[17]D. J. Chadi, Phys. Rev. B **16**, 790 (1977).

[18]R. Hill, J. Phys. C **7**, 516 (1974).

[19]A. P. Litvinchuk and N. I. Vitrikhovskii, Phys. Status Solidi B **115**, K151 (1983); A. Sharmann, D. Schwabe, and D. Weyland, J. Lumin. **18-19**, 833 (1979).

[20]S. Larach, R. E. Shrader, and C. F. Stocker, Phys. Rev. **108**, 507 (1957).

[21]A. Ebina, E. Fukunaga, and T. Takahashi, Phys. Rev. B **10**, 2495 (1974).

[22]L. Soonckindt, D. Etienne, J. P. Marchand, and L. Lassabatere, Surf. Sci. **86**, 378 (1979); D. Etienne, M. de Murcia, and G. Bougnot, Thin Solid Films **70**, 285 (1980).

[23]F. F. Morehead, J. Phys. Chem. Solids **24**, 37 (1963).

[24]R. Mach, P. Flögel, L. G. Suslina, A. G. Areshkin, J. Maege, and G. Voigt, Phys. Status Solidi B **109**, 607 (1982); J. E. Nicholls, J. J. Davies, N. R. J. Podton, R. Mach, and G. O. Müller, J. Phys. Chem. **18**, 455 (1985).

[25]A. A. El Shazly, M. M. H. El Naby, M. A. Kenawy, M. M. El Nahass, H. T. El Shair, and A. M. Ebrahim, Appl. Phys. A **36**, 51 (1985).

[26]L. G. Suslina, D. L. Fedorov, S. G. Konnikov, F. F. Kodzhespirow, A. A. Andreev, and E. G. Shariai, Fiz. Tekh. Poluprovodn. **11**, 1934 (1977) [Sov. Phys.—Semicond. **11**, 1132 (1977)].

[27]R. Hill and D. Richardson, J. Phys. C **6**, L115 (1973). For the method of preparation see R. Hill and D. Richardson, Thin Solid Films **15**, 303 (1973).

[28]M. Aven and W. Garwacki, J. Appl. Phys. **38**, 2302 (1967).

[29]A. Ebina, M. Yamamoto, and T. Takahashi, Phys. Rev. B **6**, 3786 (1972).

[30]J. F. Hunter, G. Ball, and D. J. Morgan, Phys. Status Solidi

B **45**, 679 (1971).
[31]K. R. Schulze, H. Neumann, and K. Unger, Phys. Status Solidi B **75**, 493 (1976).
[32]A. Baldereschi, E. Hess, K. Maschke, H. Neumann, K. R. Schulze, and K. Unger, J. Phys. C **10**, 4709 (1977).
[33]D. Richardson, J. Phys. C **4**, L289 (1971).
[34]D. Richardson, J. Phys. C **4**, L335 (1971).
[35]R. Hill and D. Richardson, J. Phys. C **4**, L339 (1971).
[36]D. Richardson, J. Phys. C **5**, L27 (1972).
[37]R. Hill, J. Phys. C **7**, 521 (1974).
[38]J. A. Van Vechten and T. K. Bergstresser, Phys. Rev. B **1**, 3351 (1970).
[39]D. Richardson and R. Hill, J. Phys. C **5**, 821 (1972).
[40]T. P. Pearsall, in *GaInAsP Alloy Semiconductors*, edited by T. P. Pearsall (Wiley Interscience, New York, 1982), p. 295.
[41]L. Nordheim, Ann. Phys. (Leipzig) **9**, 607 (1931).
[42]A. B. Chen and A. Sher, Phys. Rev. B **22**, 3886 (1980).
[43]W. Porod, D. K. Ferry, and K. A. Jones, J. Vac. Sci. Technol. **21**, 965 (1982).
[44]P. A. Fedders and C. W. Myles, Phys. Rev. B **29**, 802 (1984).
[45]P. J. Dean, G. Kaminsky, and R. B. Zetterstrom, Phys. Rev. **181**, 1149 (1969); B. L. Joesten and F. C. Brown, *ibid.* **148**, 919 (1966); A. N. Pikhtin, V. N. Razbegaev, and D. A. Yaskov, Phys. Status Solidi B **50**, 717 (1972); N. N. Sirota, I. V. Bodnar, A. I. Lukomskii, G. F. Smirnova, and L. M. Finkelstein, *ibid.* **73**, K135 (1976).
[46](a) A. Baldereschi and K. Maschke, Solid State Commun. **16**, 99 (1975); (b) M. Altarelli, *ibid.* **15**, 1607 (1974).
[47]J. L. Martins and A. Zunger, J. Mater. Res. **1**, 523 (1986); Phys. Rev. Lett. **56**, 1400 (1986).
[48](a) G. P. Srivastava, J. L. Martins, and A. Zunger, Phys. Rev. B **31**, 2561 (1985); (b) This structure has previously been referred to as the luzonite structure [Refs. 47 and 48(a)]. However, we have since concluded that the rather confusing literature on luzonite and related minerals does not warrant this usage. We refer the reader to the following relevant discussions. F. Marumo and W. Nowacki, Z. Kristallogr. **124**, 1 (1967) and R. V. Gaines, Am. Mineral. **42**, 766 (1957), contain determinations of the structure and composition of luzonite and famatinite, together with useful historical remarks. C. B. Sclar and M. Drovenik, Bull. Geol. Soc. Am. **71**, 1970 (1960), identify a mineral (which they call lazarevićite) with the same composition as some samples of luzonite, but with the same structure we refer to here as Cu_3Au-like. We have found no corroborative work on this mineral. G. Tanelli, Atti Accad. Naz. Lincei Cl. Sci. Fis. Mat. Nat. Rend. **46**, 196 (1969), presents a phase diagram of the Cu_3AsS_4-Cu_3SbS_4 system, showing regions identified as enargite, luzonite, and famatinite, the latter two having the same crystal structure (with space group $I\bar{4}2m$), whereas the former has a wurtzitelike structure (space group $Pmn2_1$).
[49]W. E. Spicer, J. A. Silberman, J. Morgen, I. Lindau, J. A. Wilson, A. B. Chen, and A. Sher, Phys. Rev. Lett. **49**, 948 (1982); Physica **117&118B**, 60 (1983).
[50]K. E. Kirschfeld, N. Nelkowski, and T. S. Wagner, Phys. Rev. Lett. **29**, 66 (1972).
[51]A. Reznitsky, S. Permagorov, S. Verbin, A. Naumov, Yu. Korostelin, V. Novozhilov, and S. Prokovev, Solid State Commun. **52**, 13 (1984).
[52]P. Galtier, J. Chevallier, M. Zigone, and C. Martinez, Phys. Rev. B **30**, 726 (1984); E. Bedel, R. Carles, A. Zwick, J. B. Renucci, and M. A. Renucci, *ibid.* **30**, 5923 (1984); R. Beserman and D. Schmeltzer, Solid State Commun. **24**, 793 (1977).
[53]H. G. Grimmeiss, E. Meijer, R. Mach, and G. O. Müller, J. Appl. Phys. **56**, 2768 (1984).
[54]L. Samuelson, S. Nilsson, Z. G. Wang, and H. G. Grimmeiss, Phys. Rev. Lett. **53**, 1501 (1984).
[55]A. Willig, B. Sapoval, K. Leibler, and C. Vèrié, J. Phys. C **9**, 1981 (1976).
[56]A. Zunger and J. E. Jaffe, Phys. Rev. Lett. **51**, 662 (1983).
[57]J. E. Jaffe and A. Zunger, Phys. Rev. B **29**, 1882 (1984).
[58]D. M. Wood, S.-H. Wei, and A. Zunger, Phys. Rev. Lett. **58**, 1123 (1987).
[59]S.-H. Wei and A. Zunger, Phys. Rev. Lett. **56**, 2391 (1986).
[60]J. C. Mikkelsen and J. B. Boyce, Phys. Rev. Lett. **49**, 1412 (1982); Phys. Rev. B **28**, 7130 (1983); *ibid.* **31**, 6903 (1985).
[61]N. Motta, A. Balzarotti, P. Letardi, A. Kisiel, M. T. Czyzyk, M. Zimnal-Starnawska, and M. Podgorny, Solid State Commun. **53**, 509 (1985); A. Balzarotti, N. Motta, A. Kisiel, M. Zimnal-Starnawska, and M. T. Czyzyk, Phys. Rev. B **31**, 7526 (1985).
[62]J. L. Martins and A. Zunger, Phys. Rev. B **30**, 6217 (1984). A similar calculation, retaining only the leading term (bond stretching) in the expression of Martins and Zunger was subsequently published by C. K. Shih, W. E. Spicer, W. A. Harrison, and A. Sher, Phys. Rev. B **31**, 1139 (1985). Their result gives only the first term in the more general expression given previously by Martins and Zunger which incorporates both bond-stretching and bond-bending effects.
[63]M. L. Cohen and V. Heine, in *Solid State Physics*, edited by H. Ehrenreich, R. Seitz, and D. Turnbull (Academic, New York, 1970), Vol. 24, p. 38.
[64]M. L. Cohen, Science **179**, 1189 (1973).
[65]V. Heine and R. O. Jones, J. Phys. C **2**, 719 (1969); P. Y. Yu and M. Cardona, Phys. Rev. B **2**, 3193 (1970).
[66]D. J. Chadi and M. L. Cohen, Phys. Status Solidi B **68**, 49 (1975) represented band states in a form that can be Taylor expanded to give Eq. (12), i.e., for the top of the valence band in zinc-blende semiconductors

$$E(\Gamma_{15v})=\{(\varepsilon_p^C+\varepsilon_p^A)/2+[(\varepsilon_p^C-\varepsilon_p^A)/2]^2+4E_{pp}^2\}^{1/2},$$

$$E(\Gamma_{1c})=\{(\varepsilon_s^C+\varepsilon_s^A)/2-[(\varepsilon_s^C-\varepsilon_s^A)/2]^2+4E_{ss}^2\}^{1/2}.$$

Here A and C denote the anion and cation, respectively, ε_α denotes the orbital energies ($\alpha=s,p$), and $E_{\alpha\alpha}$ the coupling matrix element.
[67]The following papers describe almost equally good tight-binding fits to the observed band structures of zinc-blende semiconductors, using *completely different* fitting parameters [analogous to V, U, and W of Eq. (12)]: S. Das Sarma and A. Madhukar, Phys. Rev. B **24**, 2051 (1981); S. N. Sahu, J. T. Borenstein, V. A. Singh, and J. W. Corbett, Phys. Status Solidi B **122**, 661 (1984); P. Vogl, H. P. Hjalmarson, and J. D. Dow, J. Phys. Chem. Solids **44**, 365 (1983); W. Porod and D. K. Ferry, Phys. Rev. B **27**, 2587 (1983); A. B. Chen and A. Sher, *ibid.* **22**, 3886 (1980). See also recent discussions on the nonuniqueness of this tight-binding approach by A. B. Chen and A. Sher, Phys. Rev. B **31**, 6490 (1985). EPM fits to the observed spectra are likewise nonunique: only if the number of pseudopotential form factors is drastically truncated (to 2 or 3 per atom; see Ref. 63) then the problem is made "unique."
[68]A. B. Chen and A. Sher, Phys. Rev. B **23**, 5360 (1981); Phys. Rev. Lett. **40**, 900 (1978).
[69]M. Bugajski, A. M. Kontkiewicz, and H. Mariette, Phys. Rev. B **28**, 7105 (1983).
[70]H. Ehrenreich and K. C. Hass, J. Vac. Sci. Technol. **21**, 133 (1982).

[71]D. Z.-Y. Ting and Y.-C. Chang, Phys. Rev. B **30**, 3309 (1984).
[72]T. Mizutani and K. Hirose, Jpn. J. Appl. Phys. **24**, L119 (1985).
[73]R. Kikuchi, Phys. Rev. **81**, 988 (1951).
[74]A. A. Mbaye, L. G. Ferreira, and A. Zunger, Phys. Rev. Lett. **58**, 49 (1987).
[75]L. D. Landau and E. M. Lifshitz, *Statistical Physics* (Pergamon, Oxford, 1969), Chap. 14.
[76]A. G. Khachaturyan, *Theory of Structural Transformations in Solids* (Wiley, New York, 1983).
[77]For $GaAlAs_2$ in the CuAu I structure see T. S. Kuan, T. F. Kuech, W. I. Wang, and E. L. Wilkie, Phys. Rev. Lett. **54**, 201 (1985). For Ga_2AsSb in the chalcopyrite structure see H. R. Jen, M. J. Cherng, and G. B. Stringfellow, Appl. Phys. Lett. **48**, 1603 (1986), and for $InGa_3P_4$ and In_3GaP_4 in the famatinite structure see H. Nakayama and H. Fujita, in *GaAs and Related Compounds, 1985, Karuizawa, Japan,* edited by M. Fujimoto (Adam Hilger, Bristol, England, 1986), p. 289.
[78]J. L. Martins and A. Zunger, Phys. Rev. B **32**, 2689 (1985).
[79]G. Martinez, in *Handbook of Semiconductors,* edited by M. Balkanski (North-Holland, Amsterdam, 1980), p. 181; A. Blancha, H. Presting and M. Cardona, Phys. Status Solidi B **126**, 11 (1984).
[80]J. C. W. Folmer and H. F. Franzen, Phys. Rev. B **29**, 6261 (1984).
[81]D. G. Seiler and K. L. Hatcox, Phys. Rev. Lett. **29**, 647 (1972); W. Pötz and P. Vogl, Phys. Rev. B **24**, 2025 (1981).
[82]P. Bendt and A. Zunger, Phys. Rev. B **26**, 3114 (1982).
[83]D. Ceperley and B. J. Alder, Phys. Rev. Lett. **45**, 566 (1980).
[84]J. P. Perdew and A. Zunger, Phys. Rev. B **23**, 5048 (1981).
[85]D. M. Wood and A. Zunger, J. Phys. A **18**, 1343 (1985).
[86]For some of the early discussions of the "band-gap problem" in local density, see A. Zunger, J. Vac. Sci. Technol. **16**, 1337 (1979); A. Zunger and A. J. Freeman, Phys. Rev. B **16**, 2901 (1977).
[87]Presented by J. B. Boyle and J. C. Mikkelson, in *Ternary and Multinary Compounds: Proceedings of the Seventh International Conference,* edited by S. Deb and A. Zunger (Materials Research Society, Pittsburgh, 1987).
[88](a) A general discussion of folding and interaction effects (applied to the chalcopyrite system) is given by D. J. Morgan, Phys. Status Solidi B **48**, 771 (1971). (b) The symmetry notations are given by R. H. Parmenter, Phys. Rev. **100**, 573 (1955).
[89]S.-H. Wei and A. Zunger (unpublished).
[90]C. S. Wang and B. M. Klein, Phys. Rev. B **24**, 3393 (1981).
[91]D. J. Stukel, R. N. Euwema, T. C. Collins, F. Herman, and R. L. Kortum, Phys. Rev. **179**, 740 (1969).
[92]F. Herman, R. L. Kortum, C. D. Kuglin, and J. L. Shay, in *II-VI Semiconducting Compounds,* edited by D. G. Thomas (Benjamin, New York, 1967), p. 503; F. Herman, R. L. Kortum, C. D. Kuglin, J. P. Van Dyke, and S. Skillman, in *Methods of Computational Physics* (Academic, New York, 1968), p. 193.
[93]P. Eckelt, O. Madelung, and J. Treusch, Phys. Rev. Lett. **18**, 656 (1967); J. Treusch, P. Eckelt, and O. Madelung, in *II-VI Semiconducting Compounds,* edited by D. G. Thomas (Benjamin, New York, 1967), p. 558.
[94](a) J. R. Chelikowsky and M. L. Cohen, Phys. Rev. B **14**, 556 (1976); (b) R. M. Wentzcovitch, S. L. Richardson, and M. L. Cohen, Phys. Lett. **114A**, 203 (1986).
[95]J. R. Chelikowsky, D. J. Chadi, and M. L. Cohen, Phys. Rev. B **8**, 2786 (1973).
[96](a) J. D. Joannopoulos and M. L. Cohen, J. Phys. C **6**, 1572 (1973); (b) M. L. Cohen, Science **179**, 1189 (1973); (c) J. P. Walter and M. L. Cohen, Phys. Rev. B **4**, 1877 (1971).
[97]J. P. Walter, M. L. Cohen, Y. Petroff, and M. Balkanski, Phys. Rev. B **1**, 2662 (1970).
[98]R. A. Pollak, L. Ley, S. P. Kowalczyk, D. A. Shirley, J. Joannopoulos, D. J. Chadi, and M. L. Cohen, Phys. Rev. Lett. **29**, 1103 (1973); L. Ley, R. A. Pollak, F. R. McFeely, S. P. Kowalczyk, and D. A. Shirley, Phys. Rev. B **9**, 600 (1974).
[99]W. D. Gorbman, and D. E. Eastman, Phys. Rev. Lett. **29**, 1508 (1972); D. E. Eastman, W. D. Grobman, J. L. Freeouf, and M. Erbudak, Phys. Rev. B **9**, 3473 (1974).
[100]D. Theis, Phys. Status Solidi B **79**, 125 (1977).
[101]M. Cardona and D. L. Greenaway, Phys. Rev. **131**, 98 (1963).
[102]J. W. Baars, in *II-VI Semiconducting Compounds,* edited by D. G. Thomas (Benjamin, New York, 1967), p. 631.
[103]B. Segall and D. T. F. Marple, in *Physics and Chemistry of II-VI Compounds,* edited by M. Aven and J. S. Prener (North-Holland, Amsterdam, 1967), p. 319.
[104]Y. Petoff, M. Balkanski, J. P. Walter, and M. L. Cohen, Solid State Commun. **7**, 459 (1969).
[105]W. A. Harrison, *Electronic Structure and the Properties of Solids* (Freeman, San Francisco, 1980), p. 155, Fig. 6.8.
[106]D. M. Wood, A. Zunger, and R. de Groot, Phys. Rev. B **31**, 2570 (1985).
[107]S. P. Kowalczyk, J. T. Cheung, E. A. Kraut, and R. W. Grant, Phys. Rev. Lett. **56**, 1605 (1986).
[108]J. Tersoff, Phys. Rev. Lett. **56**, 2755 (1986), and references therein.
[109]T. Yamanaka and M. Tokonami, Acta Crystallogr. B **41**, 298 (1985).
[110]P. M. Raccah, R. N. Euwema, D. J. Stukel, and T. C. Collins, Phys. Rev. B **1**, 756 (1970).
[111]D. W. Langer, R. N. Euwema, K. Era, and T. Koda, Phys. Rev. B **2**, 4005 (1970).
[112]B. A. Weinstein, R. Zallen, M. L. Slade, and A. De Lozanne, Phys. Rev. B **27**, 4652 (1981).
[113]A. L. Edwards, T. E. Slykhouse, and H. G. Drickhamer, J. Phys. Chem. Solids **11**, 140 (1959).
[114]A. Zunger, Int. J. Quantum Chem. **195**, 629 (1986), has used less-stringent convergence criteria in the band-structure calculations, resulting in $b_S = 0.93$ eV and $b_I = 1.33$ eV instead of 1.32 and 1.96 eV, respectively, reported here (Table XII).
[115]M. Caldas, A. Fazzio, and A. Zunger, Appl. Phys. Lett. **45**, 671 (1984).
[116]A. Zunger, in *Solid State Physics,* edited by H. Ehrenreich and D. Turnbull (Academic, New York, 1986), Vol. 39, Sec. VI.29, p. 275.
[117]W. D. Laidig, N. Holonyak, J. J. Coleman, and P. D. Dapkus, J. Electron. Mater. **11**, 1 (1982).